Thermodynamics of Fe-Mg olivines at mantle pressures: Mid- and far-infrared spectroscopy at high pressure*

A. M. Hofmeister,** J. Xu,** H.-K. Mao, P. M. Bell, T. C. Hoering

Geophysical Laboratory, Carnegie Institution of Washington, 2801 Upton Street, N.W., Washington, D.C. 20008, U.S.A.

Abstract

The first far-IR spectra of silicates at high pressure have been obtained by combining various state-of-the-art technologies. Three olivines (Fo_{100}, Fo_{87}, and Fo_0) were studied at pressures of up to 425 kbar. In addition, mid-IR data on Fo_{100} were obtained up to 240 kbar. The same pressure responses (i.e., changes in peak position, area, etc.) were seen in the hydrostatic and nonhydrostatic experiments. By augmenting these data with mid-IR studies at pressure by Xu et al. (1983), all IR modes in Mg-Fe olivines are characterized as a function of pressure. The data corroborate the band assignments for olivine and the correlation of the forsterite and fayalite 1-atm spectra by Hofmeister (1987), in that similar behavior with pressure is observed for analogous bands in these minerals, with each different type of vibrational motion having a distinct pressure response. The response to pressure of bands assigned to SiO_4 vibrations differs fundamentally from that of bands involving M ions in a manner that is consistent with the relative incompressibility of the SiO_4 tetrahedron. A gradual transformation from olivine to a more symmetric structure is supported by the generally continuous but individual responses of peak area and frequency to pressure, by the appearance of new bands at pressure, and by the occurrence of mode softening.

Initial values for the first mode Grüneisen parameter ($\gamma_i \equiv -\partial \ln \nu_i/\partial \ln V$) range from 0.10 to 2.0 such that far-IR modes (translations or rotations) generally have values larger than unity, whereas mid-IR modes (internal vibrations) all have values less than unity. At pressures significantly above the stability field of olivine, γ_i can become negative. Within the olivine stability field, γ_i is nearly constant for the majority of the IR bands. The strong curvature of frequency with pressure, occurring for four to six modes for each mineral, allows accurate determination of not only the first but also the second Grüneisen parameter ($q_i \equiv d \ln \gamma_i/d \ln V$), such that $q_i(0)$ ranges from zero to nine. It is not clear that integer values are required. Modes with $q_i(0)$ greater than six have an appreciable pressure dependence of q_i, suggesting that constant q_i is not appropriate for the other bands. For the majority of bands, which do not exhibit curvature of frequency with either pressure or volume, $\gamma_i(0)$ can be determined within $\pm 20\%$ and $q_i(0)$ can be estimated as roughly -1.5 ± 3.0, by averaging values determined from polynomial fits of $\nu(V)$ and $\nu(P)$. The negative q_i values are mandated by the linear dependence of ν on P. These large uncertainties result from the interdependence of γ_i and q_i and are commonly and incorrectly ignored in computing Grüneisen parameters.

Introduction

Thermochemical characterization of high-pressure phases is essential to describe the phase relations and the thermal structure of the Earth's mantle. Without extensive thermochemical and lattice-dynamics data, models of the mantle remain poorly constrained (e.g., Lees et al., 1983). At the present, heat capacity cannot be measured by performing calorimetry at pressure, but this problem can be circumvented by measuring vibrational spectra of minerals at mantle pressures and by utilizing these data to calculate heat capacity and entropy as a function of both temperature and pressure (see Kieffer, 1979a, 1979b, 1979c, 1980, 1982). Furthermore, the mode Grüneisen parameters (γ_i) obtained from the same experiments permit direct calculation of γ_{th} as a function of pressure.

High-pressure Raman and mid-IR studies have been performed on a wide variety of solids and liquids [see reviews by Sherman (1982) and Ferraro (1984)]. In particular, mid-IR spectra taken from magnesian olivine to 50 kbar (Dietrich and Arndt, 1982) and from forsterite and fayalite to 300 kbar (Xu et al., 1983) have frequencies

---

(v) that increase linearly with pressure at rates of 0.08 to 0.5 cm^{-1}/kbar. The high-energy Raman bands of forsterite have similar slopes of 0.3 cm^{-1}/kbar (Besson et al., 1982). However, to date, far-IR spectroscopy ($v < 300$ cm^{-1}) has been limited to low pressures (<60 kbar) and to a few classes of solids, mainly halides (e.g., Ferraro et al., 1966, 1971a; Lowndes and Rastogi, 1976; Shawyer and Sherman, 1982). At these moderate pressures, the vibrational frequencies depend linearly on pressure, except that dv/dP of potassium halides decreases steadily with pressure (Ferraro et al., 1971b) and dv/dP of ZnS has a slight initial curvature (Ferraro et al., 1970). The only oxide studied so far (TeO$_2$) showed an increase in frequency with pressure and splitting of a band at a second-order phase transition (Adams and Sharma, 1978).

Olivine is a prime candidate for study by high-pressure far-IR spectroscopy because (1) it is likely to be a major constituent of the upper mantle, (2) band positions and assignments at ambient pressure are established (Hofmeister, 1987), (3) Kieffer's (1979c) lattice-dynamics model accurately reproduces heat capacity C_v and entropy S at 1 atm for forsterite (Akaogi et al., 1984) and fayalite (Hofmeister, 1987), (4) the behavior of Raman bands at pressure is expected to parallel that of the IR bands since both sets of bands are derived from the same atomic motions, and (5) the pressure dependences of the other properties needed to compute $C_v(P)$ are known or can be computed.

This paper presents the first far-IR (370–80 cm^{-1}) spectra of any substance above 60 kbar and of any silicate at pressure. Synthetic forsterite and natural Fo$_{87}$ and fayalite were studied at hydrostatic and nonhydrostatic pressures of up to 425 kbar, and mid-IR spectra of synthetic forsterite crystals were obtained at quasi-hydrostatic pressures of up to 240 kbar. Innovations needed to perform these experiments are described. The response of band areas to pressure is used to evaluate changes in bonding and structure. The change of vibrational frequencies with pressure is used to evaluate band assignments based on 1-atm spectra. Mode Grüneisen parameters ($\gamma_i \equiv -d \ln v_i/d \ln V$) and their derivatives ($q_i \equiv d \ln \gamma_i/d \ln V$) are computed and compared. In a subsequent paper, the mode Grüneisen parameters will be averaged, compared to γ_{th} at 1 atm, and used to predict the pressure dependence of γ_{th}. The pressure dependence of heat capacity and the other energy variables will be predicted by applying Kieffer's model to $v(P)$. These data will then be used to calculate a geotherm for the Earth's upper mantle that can be compared directly to geotherms computed from seismic data.

EXPERIMENTAL DETAILS

Obtaining far-IR spectra at very high pressures requires a unique combination of technologies: a Fourier-transform IR spectrometer, a liquid-He–cooled bolometer, a custom-designed beam-condenser, and a megabar diamond-anvil cell (DAC). A detailed description of the ex-

perimental techniques is given for the nonstandard procedures.

Four samples were studied: (1) forsterite powder synthesized by H.-K. Mao; (2) single-crystal forsterite grown by the Czochralski technique at Union Carbide; (3) natural olivine (Fo$_{87}$) from Balsam Gap, North Carolina, containing a significant amount of Fe (7.17 wt% as FeO: App. Table 1),[1] but negligible amounts of other elements likely to occur in olivine; and (4) natural fayalite from Inyo County, California, essentially devoid of Mg (App. Table 1), but containing 6 mol% Mn$_2$SiO$_4$. The effect of such small amounts of Mn can be ignored because the fayalite-tephroite series exhibits little change in the far-IR spectra at low Mn concentrations (Kovach et al., 1975).

Pressures were generated by a megabar DAC as described by Mao and Bell (1978) and gauged by the shift of the R_1 fluorescence line of ruby (Mao et al., 1978) by means of an automated scanning spectrometer (Mao et al., 1983). Hydrostatic pressures were corrected as described by Jephcoat et al. (1986) using the calibration of Mao et al. (1986).

Sample configuration is critical for obtaining data. In one set of experiments, single crystals of natural olivine were loaded nonhydrostatically in a sandwich configuration (Fig. 1A). Polyethylene was pressed into a 150-μm-radius aperture that was drilled into an Inconel gasket preindented to 150 kbar; a single-crystal slab 20–30 μm thick and >150 μm in radius was laid on top of the gasket; and micrometer-sized ruby chips were scattered over the sample. The large sample thickness was needed to resolve the weak lowest-energy mode. A large aperture is needed to compensate for low light intensity (see below). Application of pressure forced the crystal into the polyethylene-filled aperture (Fig. 1B). Below 100 kbar, pressure gradients were small (~20 kbar over 150 μm), but at the highest pressures attained (320 kbar), gradients were large (~150 kbar over 220 μm). Large pressure gradients were not a problem in analyzing the results because the far-IR bands change slowly with pressure. The thickness of the fayalite crystal decreased from about 25 to 10 ± 1 μm over the course of these experiments.

Powdered forsterite was loaded in a similar sandwich configuration for nonhydrostatic runs (Fig. 1C). Petroleum jelly was used as the medium for similar experiments on powdered fayalite. The aperture was covered by very fine grained ruby powder to more accurately measure pressure.

For comparison, synthetic forsterite powder was measured under *hydrostatic* conditions. Fo$_{100}$ was compressed to form a thin film (~5 μm) on one anvil. Ruby powder was then fixed similarly to the other anvil. A gasket predrilled at 250-μm diameter was placed between the two
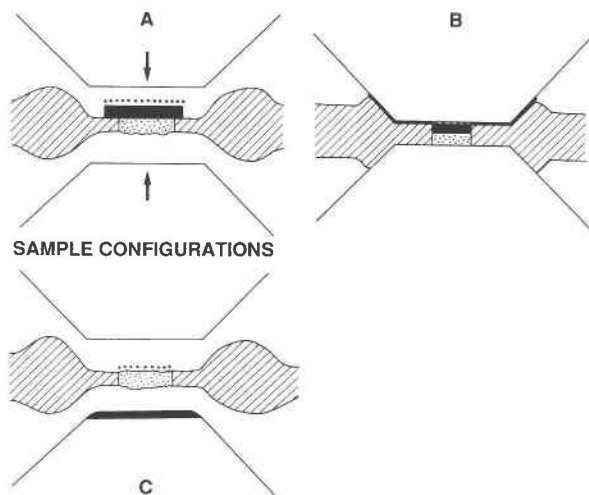
Fig. 1. Sample configurations. Cross-sectional views of diamond anvils, showing the gaskets (diagonal lines), pressure media (stippled area), olivine sample (solid black), and ruby crystals (dots). (A) Nonhydrostatic single-crystal experiments. The gasket hole was filled with polyethylene, and the crystal was placed over the entire aperture. Ruby powder was scattered upon the olivine. (B) Upon compression, the olivine on the gasket was smashed while the remaining crystal sank in the polyethylene. (C) Nonhydrostatic powder experiments. A thin film of sample was made by compressing the sample between two ungasketed diamonds. The gasket aperture was filled with polyethylene (far-IR) or CsI (mid-IR) and ruby crystals were scattered on top. For hydrostatic experiments, a thin film of sample was produced as in (C) while a thin film of ruby was made similarly for the cylinder diamond. The DAC was flooded with Ar gas in a pressurized container while the diamonds were seated and compressed as described by Jephcoat et al. (1986).
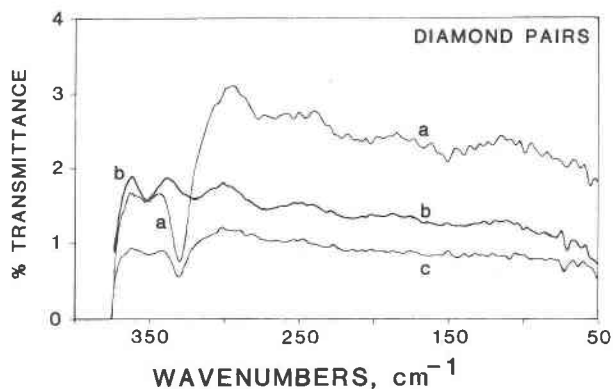

Fig. 2. Spectra of diamond pairs used as backgrounds. (a) Type I diamond pair of total thickness 4.64 mm and diameter 0.73 mm. (b) Type II diamond pair with total thickness of 2.78 mm and diameter of 0.62 mm. (c) Type I diamond pair with total thickness 4.84 mm and diameter of 0.62 mm. The transmittance of a given diamond is apparently sample specific.

anvils; then the sample chamber was flooded with Ar in a gas bomb, and the cell was initially pressurized to about 40 kbar. During this process, the aperture constricted to 160-μm diameter. The aperture steadily increased to about 250-μm diameter during the compression runs. The errors in pressure were determined within $\pm2\%$ by making 12 to 40 measurements of the shifts in the ruby line at each pressure increment.

Spectra were acquired at resolutions of 4 cm^{-1} in a Nicolet 7199 Fourier-transform infrared (FTIR) spectrometer equipped with a liquid-He–cooled bolometer (Infrared Laboratories Inc.) of frequency range 370–70 cm^{-1} with a sensitivity D^* of 1.2×10^{12} cm·Hz$^{1/2}$W^{-1}. Despite the high sensitivity of this detector, obtaining far-IR spectra was not possible without the addition of an all-reflecting beam condenser (App. Fig. 1) that quadrupled the through-put.

The three pairs of diamond anvils used in these experiments varied widely in their absorbances (Fig. 2). If absorbance is normalized for both thickness and area, then the two pairs of type I diamonds are equal in absorbance and are one-half as absorbant as the type IIA pair. For mid-IR spectroscopy, only type II is usable.

Aperture size is restricted by the low light intensities in the far IR. The signal-to-noise ratio must be greater than about 1.1 for the FTIR instrument to coherently add spectra. This requirement limits aperture radius to $> \sim150$ μm for the less transparent diamond pairs and to about 100-μm radius for the most transparent diamond pair (Fig. 2), loaded with samples that absorb nearly 50% of the light. Sample thicknesses needed to obtain data on the weak lowest-energy peak in olivine absorb $\sim80\%$ of the light and thus require the use of ~200-μm apertures.

Far-IR spectra were acquired and manipulated as follows. Typical run conditions of 2000–2500 scans at a bolometer gain of 200, instrument gain of 64–128, and mirror velocity of ~0.56 cm/s allowed collection of a spectrum with an adequate signal-to-noise ratio within 1 h. The Fourier-processed data were ratioed to a spectrum of an empty DAC to give a transmission spectrum. For the thickest samples, the baseline was adjusted through the computer software to have 0% transmission at 315 cm^{-1}, at which point the 20-μm olivine crystal is opaque.

Water-vapor rotational bands (Fig. 3) were subtracted from absorbance spectra, because (1) the purging rate of the instrument varies strongly with relative humidity, (2) the absolute transmittance through the DAC is low (<1%), and (3) silicate peaks are weak whereas H$_2$O peaks are strong so that a miniscule amount of water can distort the olivine spectra. In particular, the intense sharp water vapor peaks at 305, 280, 250, 230, 205, 150, 140–120, and 100 cm^{-1} (Fig. 3; see also Moller and Rothschild, 1970) interfere with the olivine spectra so that weak features at these positions are always suspect.

Baselines were estimated visually. Widths reported are full widths at half height. Integrated intensities were approximated as the product of peak width and height (intensity). Positions of the lowest-energy peak were taken from transmission spectra in order to obtain the highest accuracy possible.

TABLE 1. Band positions and assignment for single-crystal and powder IR spectra of forsterite and fayalite

Peak	Sym-metry	Fo$_{100}$* ν	Fo$_{87}$ ν	Fo$_0$ ν	Forsterite** ν_{TO}	ν_{LO}	Fayalite** ν_{TO}	ν_{LO}	Assignment**
1	$B_{2u}(1)$	144	138†	107.5†	141.8	143.8	105.6	nd	T(SiO$_4$) + ?T(M2)
2 a	$B_{3u}(1)$	201	198†		200.8	201.4	nd	nd	T(SiO$_4$) + ?T(M1)
3 a	$B_{1u}(1)$	275	270†		275.7	275.9	168	172	
b	$B_{2u}(2)$			172†	268 ± 2	276	170	171.8	T(M2)
c	$B_{3u}(2)$			172†	274.8	276	170	174.9	
4 a	$B_{1u}(2)$	295	290†		293	299.4	180	184.9	
b	$B_{2u}(3)$			183†	290 ± 2	298 ± 2	180	183.6	T(M1)
c	$B_{3u}(3)$			183‡	293.7	297.8	180	182.9	
5	$B_{1u}(3)$			197.6*	309	313.0	191.5	199.3	
6 a	$B_{2u}(4)$			230†	300	307.6	~206	~235	T(M1)
b	$B_{3u}(4)$				309.1	313.1	205	223	
7	$B_{3u}(5)$	320			319.3	321	nd††	nd††	T(M2)
8 a	$B_{2u}(5)$	362		250†	345 ± 8	375‡	246	257	T(M2)
b	$B_{1u}(4)$				365‡	371‡	241	252	T(M1)
c	$B_{3u}(6)$				377‡	388 ± 2‡	249	258	R?‡‡
9 a	$B_{2u}(6)$	415		290*	398 ± 4‡	408 ± 4	270	325	T(M1)
b	$B_{3u}(7)$				405 ± 5	430 ± 10	278	340	T(M1)
c	$B_{1u}(5)$				412 ± 2	450	280	341	R?
10 a	$B_{2u}(7)$				418 ± 2	438.5	346	360	R
b	$B_{3u}(8)$				434 ± 4	463.2	349	385	ν_2
c	$B_{1u}(6)$	480			463 ± 3	482	366	387	R
11	$B_{2u}(8)$		505§	477§§	452 ± 2	488 ± 4	458	477.5	ν_2
12 a	$B_{3u}(9)$				505	511	~450#	~520#	ν_4
b	$B_{1u}(7)$				502.3	538 ± 3	430##	441##	ν_2
13	$B_{2u}(9)$			507§§	504 ± 2	511	498.9	529	ν_4
14	$B_{1u}(8)$	545	526§		543	573 ± 2	457##	523##	ν_4
15	$B_{2u}(10)$				520.4	572	544	595.5	ν_4
16 a	$B_{3u}(10)$	609	596§	557§§	600.8	644	542#	597.9#	ν_4
17 a	$B_{2u}(11)$	836	842§	827§§	828 ± 2	844	819	830.5	ν_1
b	$B_{3u}(11)$				840.8	842 ± 2	819	830.2	ν_1
18 a	$B_{1u}(9)$	878	884§	875§§	865 ± 5	957	850	915	ν_3
b	$B_{2u}(12)$				865 ± 5	961	864	917.8	ν_3
19	$B_{3u}(12)$	925	955§	916§§	950.1	961	867	920	ν_3
20 a	$B_{2u}(13)$	989	980§	950§§	983.6	996	938.4	958.9	ν_3
b	$B_{3u}(13)$				987.5	991	939.6	958	ν_3
overtones									
2 b	B_{2g}	245	242		244				Raman T(M2)
15 b	$B_{3u}(X)$				~575	~575			
16 b	$B_{1u}(X)$	698		675?	~610	~675			
c	$B_{2u}(X)$				~675	~650			
18 c	$B_{3u}(X)$				~873	885 ± 5			overtone
21	$B_{1u}(X)$				986	999	938	961	
22 a	$B_{1u}(X)$				1071	1087			
b	$B_{2u}(X)$			975	1071	1087	972	1018	
c	$B_{3u}(X)$				1030 ± 70	1080	966	1016	

Note: Peak correspondences are from Hofmeister (1987). nd, not detected. B_{1u}, **E** ∥ z. B_{2u}, **E** ∥ y. B_{3u}, **E** ∥ x.
  * Powder in DAC.
  ** Hofmeister (1987).
  † Single crystal in DAC.
  †† For fayallite, peaks 7c and 8 may be a doublet.
  ‡ Servoin and Piriou (1973); Iishi (1978).
  ‡‡ For faylite, the assignments for these two bands may be switched or a mixture.
  § Dietrich and Arndt (1982).
  §§ Xu et al. (1983).
  # The position is uncertain owing to mixing of polarizations. The $2\nu_4$ modes in B_{3u} may be degenerate.
  ## The very weak band at 430–441 may be an artifact, in which case ν_2 is 457–490 and ν_4 LO is 490.

Mid-IR spectra were obtained similarly from synthetic forsterite crystals, because the data of Xu et al. (1983) were masked by interference fringes and extended only to 600 cm^{-1} owing to use of BaF$_2$ lenses as a beam condensor. The all-reflecting beam condensor (App. Fig. 1), type IIA diamonds, and sandwich configuration of Figure 1C were used. Sample thickness was ½ to 1 μm. Aperature diameter was 200 μm. The CsI pressure-transmitting medium produced a maximum pressure gradient of

50 kbar from edge to center. The average pressure measured was estimated within 5% by sampling approximately 50 points. Baseline corrections were unnecessary for mid-IR spectra. Interference fringes were removed from the interferogram for the 1-kbar spectra. Peak parameters were determined from standard routines and confirmed by Fourier deconvolution (Kauppinen et al., 1981). The high signal-to-noise ratio (1000:1) required, along with the amplification of sharp bands (e.g., H$_2$O
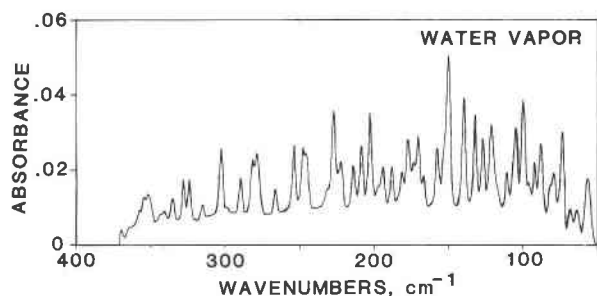
Fig. 3. Far-IR spectra of the rotational bands of water vapor. Resolution is 4 cm^{-1}. The intense bands between 300 and 100 cm^{-1} interfered with collection of the olivine spectra. In particular, the combination of H_2O bands between 225 and 235 cm^{-1} has been previously mistaken for mineral bands.

vapor) during Fourier deconvolution, prohibited application of this procedure to the far-IR data. Resolution was 2 cm^{-1} for the spectral range 4000 to 400 cm^{-1}. Run conditions were 8000 to 40000 scans at gains of 8 to 32 and mirror velocity of 1.28 cm/s.

RESULTS

The combination of mid- and far-infrared studies of olivine at pressure allowed determination of the pressure dependence of all but a few bands located near 400 cm^{-1}, the latter being in a gap between the frequency ranges of the detectors. However, *all* modes could be accounted for because analogous motions have different frequencies in forsterite and fayalite, so that every mode was measured in at least one of the end-member minerals.

High-pressure data for frequencies above 300 cm^{-1} are all from powders (Table 1). Because powder positions are an average of several modes, mostly transverse optic (TO) and, secondarily, longitudinal optic (LO), the other parameters (i.e., γ_i) are also assumed to serve as average values. In general, the combination of modes in forsterite that creates the powder spectra is the same combination that occurs in fayalite, but several exceptions occur in the middle of the spectra (400–600 cm^{-1}). This effect is accounted for in comparing forsterite to fayalite modes.

The 1-atm positions of the far-IR bands generally agree with previous work (Table 1). A very weak shoulder observed near 246 cm^{-1} for the magnesian olivines in the DAC (Tables 2, 3; App. Table 2; Figs. 4, 5; App. Fig. 2) was not found in single-crystal spectra (Hofmeister, 1987) and is likely due to excitation of a Raman band reported at 244 cm^{-1} by Iishi (1978). Single-crystal fayalite spectra at pressure (Fig. 6, Table 3) lack the 196 cm^{-1} peak, because of the orientation of B_{2u} and B_{3u} from the (100) face. Two weak shoulders present between 220 and 250 cm^{-1} match band positions for single-crystal spectra (Hofmeister, 1987), so these are unlikely to be artifacts. B_{1u} singlet 5 was obtained from powder experiments (App. Fig. 3; App. Table 3).

The 1-atm positions of the mid-IR bands agree with previous work on forsterite and resemble those of fayalite
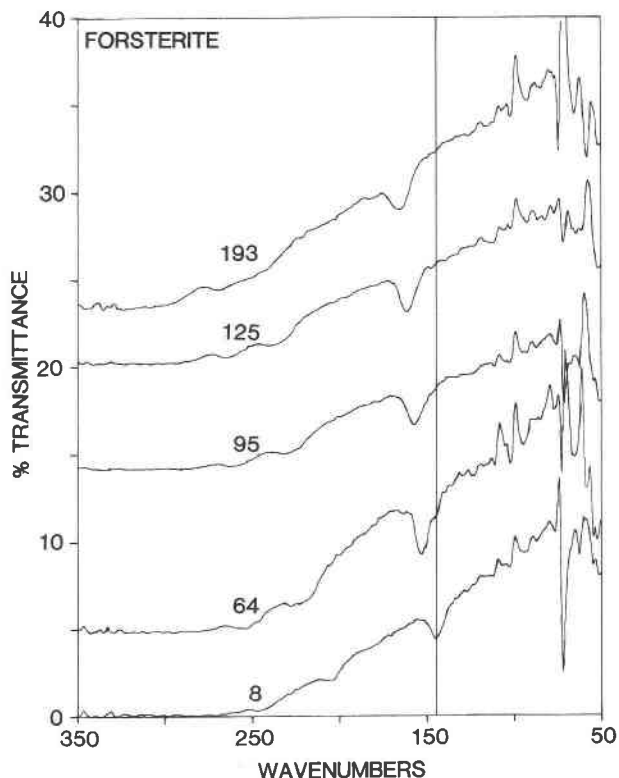

Fig. 4. Far-IR transmittance spectra of forsterite powder synthesized by H. K. Mao. Pressures are given in kbar. Spectra are offset for clarity. Except for 8 kbar, spectra were collected during compression. Accurate measurement of the parameters of the lowest-energy peak required use of a thick sample (20 μm) that was opaque at longer wavelengths so that transmittance at $\nu >$ 300 cm^{-1} is zero. The vertical line is at 147 cm^{-1}. The peaks not only shift to higher frequency with pressure, but also decrease in intensity and increase in width. The sharp peaks below 125 cm^{-1} are due to water vapor and to noise near the cutoff frequency of the beam splitter.

(App. Tables 5, 6). A weak band occurring at 700 cm^{-1} is not always present in single-crystal spectra of forsterite and fayalite; because it is in excess of the number of modes predicted by symmetry analysis (Hofmeister, 1987), it must either be an overtone, or a combination, or possibly a Si–O–Si stretching mode associated with structural changes.

Description of changes in spectra during compression

The infrared bands in olivine move to progressively higher frequencies, broaden, and decrease in intensity with pressure (Figs. 4 to 7; App. Figs. 2 and 3), regardless of Fe content, hydrostatic conditions, or band energy, with a few exceptions as discussed below. The rate of frequency increase varies among the different types of bands and approaches zero or may be slightly negative for two low-energy bands in fayalite (Fig. 6). During compression, the decrease in intensity is largely related to thinning (see below).

TABLE 2. Dependence of synthetic forsterite far-IR peak parameters on hydrostatic pressure

P (kbar):	155 ± 1	121 ± 0.5	184 ± 1	208 ± 1	234 ± 4	257 ± 2	293 ± 2
V (cm³/mol):	39.81 ± 0.018	40.51 ± 0.01	39.25 ± 0.018	38.86 ± 0.018	38.40 ± 0.045	38.04 ± 0.05	37.48 ± 0.03
λ(1)		160.9?					
λ(2a)		231?	246.9?	247.8	251 ± 2	257	
λ(2b)		273sh	278sh				
λ(3c)	301.3	297.4	303.7	305.76	308.05	310.0	312.5
Width	6		4.2	4.8	5.0	5.3	5.2
Intensity	0.19		0.19	0.21	0.181	0.175	0.156
Area	1.14		0.79	1.01	0.90	0.92	0.81
λ(3b)	311.7	306.4	317.5	320.95	323.1**	325.2**	331.3
Width	4.6		7.8 ± 0.2	7.0	7.2	8.4	<10
Intensity	0.135		0.215	0.316	0.311	0.263	0.271
Area	0.62		1.64 ± 0.04	2.24	2.23	2.18	<2.7
λ(4c)	317.2	315.3	§	§	§	§	325
Width							
Intensity							
Area							
λ(4b)	328.9	323.98	330.7 ± 0.05	332.5 ± 0.7	336.0	338.8	341.31
Width	<9.4	<10	7.2	7.4	8.0	9.6	9.6
Intensity	1.032	0.88	0.8	0.694	0.78	0.68	0.578
Area	<9.7	<8.8	5.8	5.1	6.2	6.6	5.6
λ(7)						371.2?	
Width						~2	
Intensity						0.4	
Area						~0.8	
λ(8)							

* Measured from a sample mixed in petroleum jelly on a polyethylene card.
** Sum of 3b and 4c peaks.
† Sum of 4c and 4b peaks.
§ Masked by λ(3b).

TABLE 3. Pressure dependence of fayalite far-IR peak parameters from single-crystal measurements

P (kbar):	0.001*	28 ± 4	70 ± 7	100 ± 10	135 ± 15	165 ± 18	200 ± 20	230 ± 25
V (cm³/mol):	46.39	45.44	44.20	43.42	42.62	41.99	41.32	40.77
λ(1)	107.5	108.9	112.74	114.73	117.6	118.47	119.46	119.92
Width		4.61	4.65	4.46	4.7	4.6	5.7	5.8
Intensity		0.15	0.20	0.27	0.21	0.18	0.15	0.12
Area		0.71	0.93	1.22	1.0	0.83	0.85	0.70
λ(3c)	~173	~173sh	173.78	175.2	175.74	175.36	174.86	174.52
Width	<6		~5.3	4.9	6.8	6.8	6.85	6.5
Intensity			~0.4	0.29	0.23	0.24	0.23	0.17
Area			~2.3	1.43	1.56	1.62	1.58	1.07
λ(3b)	~173	~178	181.2	185.4	187.6	188.1	~188	?
λ(4c)	183.4	190	~195	197	200	200	197.6	197.09
Width	7.7	10		15.8	20.4	28.6	<32	<38
Intensity		1.18		0.8	0.60	0.57	~0.5	~0.47
Area		11.8		12.67	12.18	16.36	<15	<16
λ(4b)	183.4	190	195.7	197	204.1	205.6	205.3	205.6
Area (3 + 4)				~13	~15	~16	~16.5	~18
λ(5)	197.6	~208	~215					
λ(6)		~232.8	~240 ± 5	239.4	246.4	251	~250?	~249?
Width				9.9	5.4	~8		
Intensity				0.08	0.04	0.04		
Area				0.8	0.2	0.3		
λ(8)	254	257	267.8	279	290	290.0	292.8	~295
Width		15.0	15.0		~28	20		
Intensity		0.58	0.63		~0.5	0.5		
Area		8.7	9.5		~14	10		

* Not measured in DAC.
† Decreasing pressure.
‡ Second increase in pressure.

TABLE 2.— Continued

328 ± 4 37.02 ± 0.05	359 ± 6 36.62 ± 0.07	425 ± 4 35.84 ± 0.04	233 ± 4 38.42 ± 0.04	91 ± 0.5 41.19 ± 0.02	62.7 ± 0.2 41.92 ± 0.01	30.8 ± 0.5 42.81 ± 0.01	7.0 ± 0.4 43.56 ± 0.01	0.001* 43.79 ± 0.01
	184 ± 1?	185 ± 2	172				145	144
				227?	~216?			201
								~246
314.43 5.1 0.146 0.74	316.3 5.4 0.137 0.74	319.96 5.8 0.118 0.68	308.2 6.2 0.113 0.70	293.5 ± 0.5	289.5sh	282.5	275sh 6.2 0.1 0.62	~275
334.6 <10 0.259 ≤2.6	336 <10 0.26 ≤2.6	341.2		302.7sh	294?		278sh ~4 ~0.1 ~0.4	~275
327.8	329	332.0 ± 2	323.4 8.2 0.195 1.60	312.3sh	308sh	302.6 19.5† 0.96† 18.7†	297.0 20† 0.96† 19.2†	295
344.0 ± 0.2 9.0 0.483 4.3	345.5 ± 0.3 9.2 0.486 4.5	348.9 ± 0.2 6.4 0.226 1.5	337.2 9.6 0.48 4.6	317.8 ± 0.5 ~20† 0.65† 13†	312.9 20† 0.89† 17.8†			295
				345.1	336.5	327.7	321	320
							>363	362

TABLE 3.— Continued

280 ± 30 39.99	320 ± 40 39.40	200 ± 30† 41.32	125 ± 15† 42.84	0 ± 1‡ 46.39
121.27 6.5 0.08 0.52	121.56 4.0 0.05 0.20	116.4	115.4	
174.12 6.5 0.10 0.67	173.4 6.2 0.07 0.43	174.3 ~0.1	172 ~6 ~0.1 ~0.6	170.5 ~5 ~0.2 ~1.0
		186.1	~184	176 ± 5
196.5 9.7 0.14 1.4	197.4 10 0.1 1.0	197.18	193.8 8.0 0.15 1.22	181.8 7.5 0.3 2.2
206.9 ~13	214 ~3		~199.7 ~1.5	~2
307 ± 3				~250

Peaks 3 and 4 (at 275 and 295 cm^{-1} in forsterite or at 173 and 183 cm^{-1} in fayalite) each split with increasing pressure. For forsterite, the higher branch of $\lambda(3)$ and the lower branch of $\lambda(4)$ are indistinguishable between 200 and 250 kbar (Figs. 5 and 8; Table 2). Above 250 kbar, the two peaks move out of Fermi resonance. The trends and relative intensities are consistent with the occurrence of a cross-over. Analogous behavior in fayalite occurs at about 130 kbar (Fig. 6, Table 3). At the highest pressure achieved (320 kbar), these peaks remain in Fermi resonance. For the natural olivine, $\lambda(3)$ and $\lambda(4)$ were not observed to split as pressure increased. The orientation of this crystal (010) would give combinations of B_{1u} ($\mathbf{E}\|x$) and B_{3u} ($\mathbf{E}\|z$) modes. If modes from these two symmetries have similar $d\nu/dP$ whereas B_{2u} ($\mathbf{E}\|y$) has different $d\nu/dP$, then splitting of peaks with pressure would be seen in powder spectra but not in spectra taken from the (010) face. That peaks 3 and 4 for natural olivine fall on the same trend as peaks 3c and 4c of forsterite (App. Fig. 4) suggests that B_{3u} is the "c" branch and B_{2u} is the "b" branch. The observed splitting of peaks 3 and 4 for the single crystal of fayalite (B_{2u} and B_{3u}) agrees with this correlation.

Assessment of experimental conditions

The forsterite data gathered under hydrostatic and nonhydrostatic conditions exhibit essentially identical
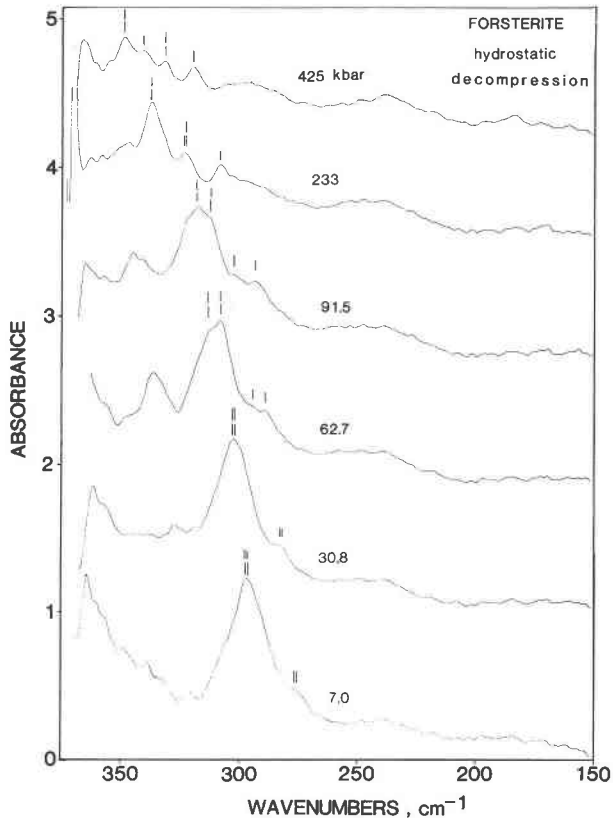
Fig. 5. Far-IR absorption spectra of synthetic Fo_{100} taken during hydrostatic decompression in an Ar matrix. Spectra are offset for clarity. The detector cuts off at about 360 cm^{-1}. A thinner sample (10–15 μm) was used in order to accurately measure peaks in the 300–400 cm^{-1} range. This precludes detection of $\lambda(1)$, except at the lowest and very highest pressures (>200 kbar), where the frequency is sufficiently separated from water-vapor bands at 150 cm^{-1}. Weak broad bands may be interference fringes. Bands 3 and 4 at 295 and 275 cm^{-1} (short dashes) were observed to shrink and split with pressure, such that the middle components merge and then cross over at high pressures.
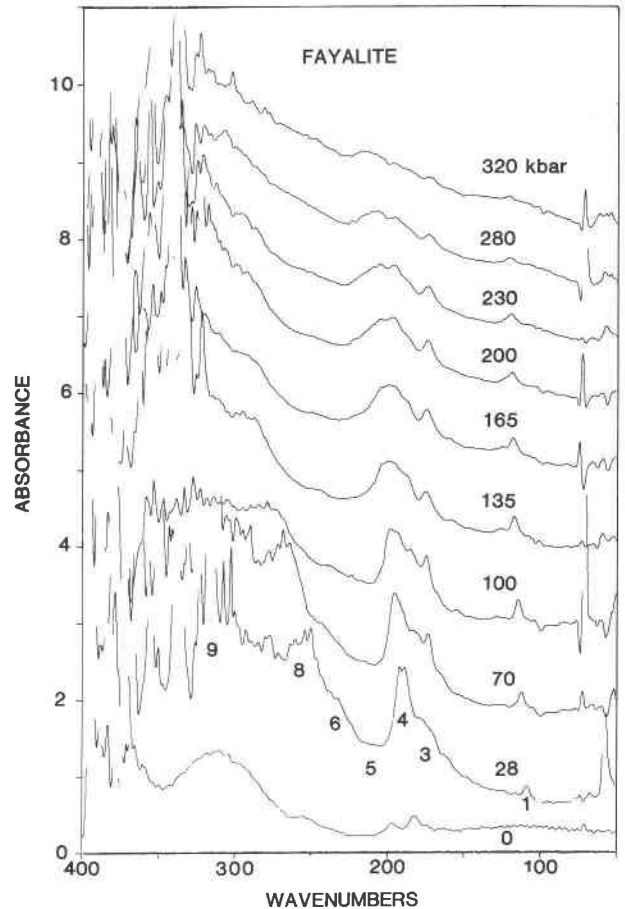

Fig. 6. Far-IR absorption spectra of single crystal of natural fayalite taken during compression. Pressures are given in kbar. The ambient pressure spectra were taken of powder in a petroleum jelly slurry on a polyethylene card. All others are from a single crystal in a DAC. Spectra are offset for clarity. All DAC spectra have about 0 absorbances near 100 cm^{-1}. Accurate measurement of the parameters of the lowest-energy peak required use of a thick sample (20 μm) that was opaque at wavelengths above 300 cm^{-1}, which causes the high-frequency noise. Spectra were baseline corrected, and water vapor was subtracted. Sharp lines below 100 cm^{-1} are due to residual water vapor.

trends of ν with pressure (Fig. 8), indicating that, at least for the mineral olivine, far-IR spectral data at pressure can be represented adequately by nonhydrostatic conditions. Hydrostatic conditions are advantageous in that the errors in pressure are one-twentieth as large, but this gain is somewhat offset by the difficulty in sample preparation. Uncertainties in pressure can be reduced for the nonhydrostatic measurements by using smaller apertures, by making separate runs over different pressure ranges, and possibly by using a different pressure medium.

Peak positions from the single-crystal fayalite experiments in polyethylene, having a large uncertainty in pressure, overlap those from the powder runs in a petroleum jelly medium (Fig. 9). The lower uncertainty in pressure and the smaller pressure gradients (50 kbar over 80 μm at 300 kbar) of the powder experiments can be attributed to the smaller aperture and to the greater coverage of ruby

crystals over the sample area rather than to different compressibilities of petroleum jelly and polyethylene.

Quantitative analysis of peak positions: Far-IR bands

The parameters of the vibrational spectra can be related to either pressure or volume. For low pressures, where volume depends linearly on pressure, similar dependencies of ν on both P and V are expected. Far-IR and mid-IR bands are discussed separately, primarily because the octahedral vibrations (exclusively located in the far-IR) and the stretching and possibly the bending modes of SiO_4 tetrahedra (the mid-IR modes) are apparently decoupled in olivine (Hofmeister, 1987).

The frequency of every far-IR band in forsterite depends linearly on pressure below 100 kbar (Fig. 8; App.
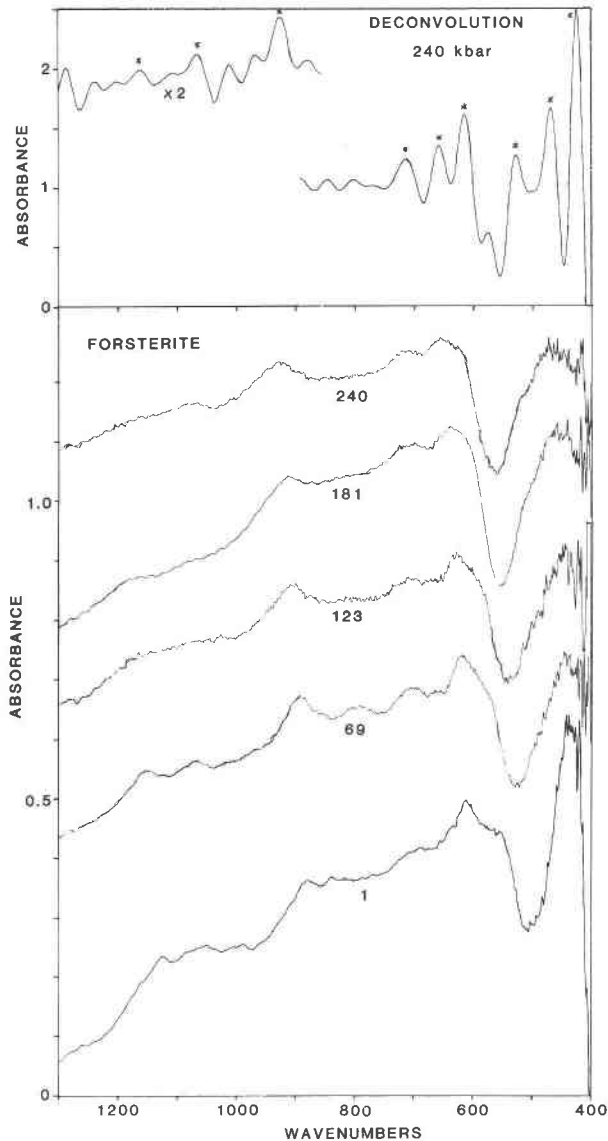
Fig. 7. Mid-IR spectra of a film of forsterite crystals taken during decompression. (Bottom) Raw data labeled by pressure in kbar. The high intensity near 450 cm^{-1} in the 1-kbar spectrum is the result of removing interference fringes and was accounted for by using a sloping baseline. In these experiments, a thick sample was used to obtain information on the weaker peaks. (Top) Fourier deconvolution of the 240-kbar spectrum using an assumed half width of 80 cm^{-1}. Peaks observable in the raw data are marked by asterisks. Other weak bands in the deconvoluted spectra may be weak interference fringes that are enhanced by the procedure. The absorbance scale at the bottom holds for all the raw spectra. Spectra are offset for clarity. All bands decrease weakly in intensity, increase in energy, and broaden as pressure increases.
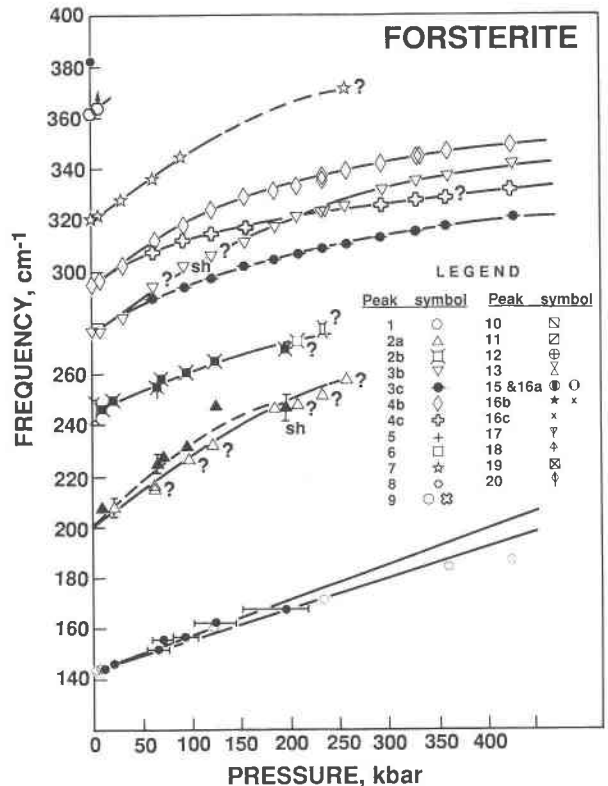

Fig. 8. Forsterite far-IR band positions as a function of pressure. Filled symbols are quasi-hydrostatic runs. Open symbols are for hydrostatic experiments. The different symbols correspond to the peaks as listed in Table 1. Except for peak 2a ($\triangle$), the frequency depends linearly on pressure for $P < 100$ kbar. Error bars in pressure are shown only for peak 1 (O). Errors in ν are less than the size of the symbol unless indicated by an error bar. The legend applies to Figs. 8–20.

Fig. 4) in agreement with previous far-IR measurements of most other materials (e.g., Ferraro, 1984; Sherman, 1982). The fayalite far-IR peak positions (Fig. 9) show linear behavior at low pressures. The absence of shear-mode softening in single-crystal elastic constants of fayal-

ite at pressures below 30 kbar (Webb et al., 1984) is compatible with the present measurements in that curvature in $d\nu/dP$ is not detectable below 50 kbar. At pressures greater than the limits of previous observations (<60 kbar), the frequencies drop below the linear trend at low pressures as the more compressible alkali halides do at lower pressure (e.g., Ferraro, 1984). This contrasts with the behavior of the mid-IR bands of forsterite with pressure wherein the frequency remains linear with pressure up to 250 kbar (Fig. 10; App. Table 7; see also Xu et al., 1983). The curvature observed for the far-IR bands (Fig. 8) is far in excess of the uncertainties of measurement. All polynomial representations of forsterite's far-IR frequencies as a function of pressure are quadratic or cubic (Table 4). The peak positions of Fo$_{87}$ exhibit similar trends (App. Fig. 4).

The peak positions of fayalite may depend linearly on pressure below 150 kbar (Fig. 9), but most show definite curvature above this pressure. As with Fo$_{100}$, the trend is toward decreasing $d\nu/dP$ with pressure. Peak 3b displays negative $d\nu/dP$ at $P > 250$ kbar, but because frequency only decreases by two wavenumbers, which is close to
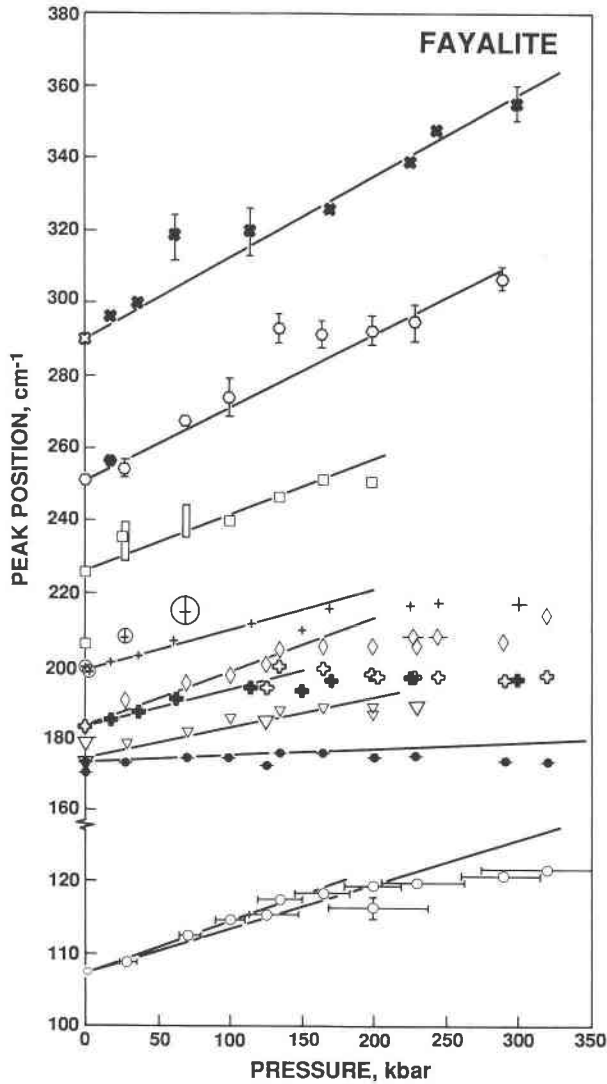
Fig. 9. Fayalite far-IR peak positions as a function of quasi-hydrostatic pressure. Symbols are listed in Fig. 8. Filled symbols represent data taken from a powdered sample. Open symbols are from the single-crystal experiments. Frequencies at pressures below 200 kbar can be fit linearly with pressure. Pressure error bars are shown only for peak 1 ($\bigcirc$). Errors in frequency are less than the size of the symbol or are indicated by error bars. Two bands ($\times$, 2 and $\bigcirc$, 4) show a decrease in frequency with pressure at $P > 150$ kbar.
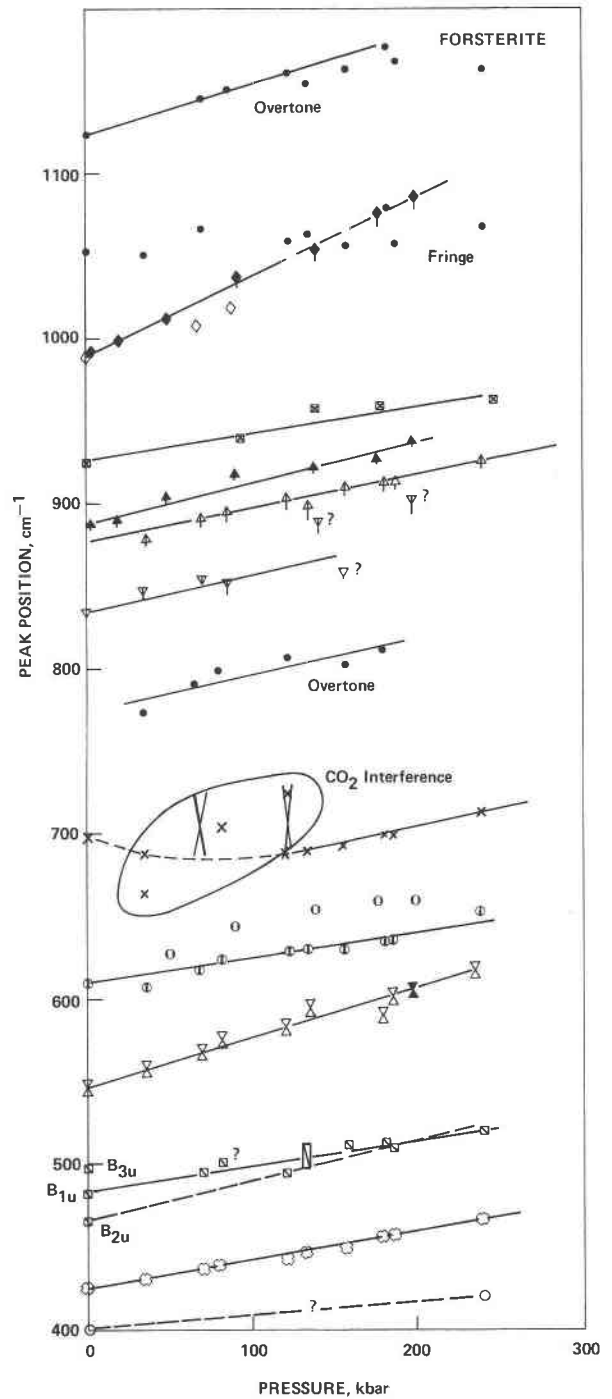

Fig. 10. Mid-IR peak positions of forsterite as a function of pressure. Symbols are listed in Fig. 8. Open symbols are data on crystals used in this study. Closed symbols are data on powder from Xu et al. (1983). The position of peak 16b ($\times$) could not be determined adequately at low pressure owing to interference by the CO_2 band at 680 cm^{-1}. Weak bands at 800 and 1050 cm^{-1} are artifacts probably resulting from unsubtracted interference fringes. The positions of bands 20 and 17 are slightly lower than the previous measurement, probably owing to interference fringes not being subtracted previously.

the experimental uncertainty, the trend may equally well be independent of P (or V). The weak peak 6 in fayalite at 225 cm^{-1} is difficult to trace with increasing pressure, because this region has several strong water bands. Polynomial representations of fayalite's frequencies as a function of pressure are quadratic or linear (Table 4). Linear fits occur for those higher-energy peaks assigned to rotations (Hofmeister, 1987) or to peaks measureable only at the lowest pressures. The lower orders occurring for the polynomial expansions for fayalite are likely related to

TABLE 4. Polynomial fits of frequency as a function of pressure

Peak no.	Fit	χ^2	ν_0	$\nu_1 P$	$\nu_2 P^2$	$\nu_3 P^3$
Forsterite						
1	Quadratic	0.19	143.90	0.1572	-1.40×10^{-4}	
2a	Quadratic	1.16	201.9	0.291	-3.19×10^{-4}	
2b	Quadratic	0.06	245.99	0.1851	-2.98×10^{-2}	
3c	Cubic	0.57	274.78	0.2631	-7.17×10^{-4}	8.39×10^{-7}
3b	Cubic	1.10	275.2	0.357	-8.62×10^{-4}	9.40×10^{-7}
4c	Cubic	0.6	295.05	0.254	-8.51×10^{-4}	1.10×10^{-6}
4b	Cubic	0.63	295.0	0.327	-8.85×10^{-4}	1.00×10^{-6}
7	Quadratic	1.5	319.62	0.300	-3.79×10^{-4}	
8	Two points		362.0	0.18		
9	Linear	0.30	426.2	0.1634		
10c + 11	Linear	0.46	482.8	0.1452		
14 + 15	Linear	0.73	547.0	0.320		
16a	Linear	0.75	608.9	0.133		
16b $P > 125$ kbar	Linear	0.09	656.7	0.240		
17	Linear	3.9	835.7	0.305		
18	Linear	0.77	876.0	0.218		
19	Linear	1.4	924.9	0.1693		
20	Linear	1.29	987.9	0.523		
Fo₈₇						
1	Quadratic	0.24	138.0	0.248	-7.84×10^{-4}	
2	Quadratic	0.44	198.3	0.477	-1.27×10^{-3}	
2b	Cubic	0.09	241.9	0.471	-4.06×10^{-3}	1.28×10^{-5}
Fo₈₄ (Dietrich and Arndt, 1982)						
12	Linear		505	0.11		
16	Linear		596	0.28		
17	Linear		842	0.21		
18	Linear		884	0.24		
19	Linear		955	0.29		
20	Linear		980	0.34		
Fayalite						
1	Quadratic	0.05	107.49	0.0770	-9.388×10^{-4}	
3c $P < 150$ kbar	Linear*	0.07	172.99	0.0151		
3b	Quadratic	0.08	173.01	0.1672	-4.87×10^{-4}	
4c	Quadratic	0.25	183.1	0.133	-3.22×10^{-4}	
4b	Quadratic	0.05	183.46	0.200	-4.05×10^{-4}	
5	Quadratic	0.39	197.50	0.164	-3.39×10^{-4}	
6	Linear	0.03	229.8	0.1173		
8	Linear	0.29	253.5	0.198		
9	Linear	0.98	291.7	0.215		
11 + 12	Linear	0.33	476.5	0.100		
15 + 16	Cubic†	0.26	558.3	0.271	-0.0104	3.8×10^{-5}
16b	Linear	0.39	620.6	0.143		
16c	Linear	0.62	697.5	0.075		
17	Linear	1.02	826.4	0.260		
18	Linear	2.31	876.4	0.251		
19	Linear	3.4	914.9	0.249		
20	Linear	0.73	948.6	0.428		
21 + 22	Linear	0.48	974.5	0.354		

* Mode softening is exhibited but the amount is too slight to influence the polynomial fit.
† For $P < 130$ kbar $\nu_0 = 558.6$ and $\nu_1 = 0.208$.

the larger uncertainties in pressure measured for fayalite than for the hydrostatic experiments of forsterite.

The correspondence of frequency with volume for the far-IR bands is linear over a much wider volume (pressure) range and has much less scatter than the correspondence of frequency with pressure. Volumes were calculated using a third-order Birch-Murnaghan equation of state. For fosterite, a bulk modulus K_T of 1280 kbar and dK_T/dP of 5.0 ± 0.4 were used (average of data from Graham and Barsch, 1969; Kumazawa and Anderson, 1969; and Kudoh and Takéuchi, 1985). For fayalite, K_T of 1265 kbar and dK_T/dP of 5.0 ± 0.4 were used (Graham et al., 1988). For natural olivine, values for K_T of 1279 kbar and dK_T/dP of 5.1 were approximated by averaging

the values of the end-members. Proportioning K and K' to Mg content is not appropriate, because the values of the end-member compositions overlap within experimental uncertainties.

For all three samples, the frequencies of peaks 2b, 7, and 9 depend linearly on volume over the entire range of pressure within the experimental uncertainty (Figs. 11, 12; App. Fig. 5; Table 5). For the synthetic forsterite, the frequencies of peaks 3 and 4 depend linearly on pressure up to 150 kbar (Fig. 11), which is approximately the stability limit of olivine with respect to the beta-spinel phase. Above 150 kbar, another straight line with lesser slope can be fit to the frequencies of peaks 3 and 4 as a function of volume. However, a more accurate representation for

TABLE 5. Polynomial fits of frequency with volume

Peak no.	Fit	x^2	a	bV	cV^2	dV^3
Forsterite						
1	Linear	1.07	378.982	−5.3832		
2a	Linear	3.13	609.264	−9.2518		
2b	Linear	3.70	521.086	−6.2851		
3ac	Cubic	0.39	2983.4	−203.049	5.2523	−0.04632
3b	Quadratic	0.9	171.177	15.4491	−0.2987	
4ac	Cubic	0.48	4221.853	−297.966	7.6715	−0.06657
4b	Quadratic	0.57	−91.976	27.8815	−0.43512	
7	Linear	1.12	720.170	−9.1534		
8	Two points		793.9	−9.86		
9	Linear	3.6	758.647	−7.70		
10c	Linear	5.0	836.841	−8.2922		
14	Linear	4.0	1096.059	−12.5856		
16a	Linear	4.4	908.175	−6.9139		
16b	Linear	1.2	776.900	−1.9655		
17	Linear	3.5	1177.713	−7.779		
18	Linear	3.6	1274.151	−9.1450		
19	Linear	9	1263.0	−7.72		
20	Linear	4.0	1872.391	−20.241		
Fo$_{87}$						
1	Linear	2.26	339.496	−4.5039		
2	Linear	3.18	668.396	−10.5696		
2b	Linear	2.99	470.133	−5.0540		
Fayalite						
1	Quadratic	0.64	−51.975	9.9973	−0.14172	
3ac	Linear	1.31	187.9085	−0.3291		
3b	Linear	1.78	298.706	−2.66		
4ac	Quadratic	2	−703.59	43.786	−0.5319	
4b	Linear	2	364.306	−3.845		
5	Quadratic	1.33	−299.9	26.86	−0.348	
6	Linear	2.1	437.98	−4.51		
8	Linear	3.07	649.745	−8.5922		
9	Linear	6	712.28	−9.0939		
11 + 12	Linear	1.9	645.688	−3.665		
13 + 14	Two points		911.5	−8.710		
16 (P < 200 kbar)	Linear	3	962.244	−8.7445		
(P > 140 kbar)	Linear	4	1279.59	−16.310		
17	Linear	3	1322.78	−10.708		
18	Linear	5.76	1396.29	−11.23		
19	Linear	6	1474.45	−12.1177		
20	Linear	5	1762.85	−17.65		

peaks 3 and 4 is the quadratic or cubic polynomials of Table 5. For the natural olivine, all frequencies follow linear trends with volume (App. Fig. 5). For fayalite, the frequencies of peaks 3 and 4 depend linearly on volume only up to 170 and 110 kbar, respectively (Fig. 12). Above these pressures, the frequencies of two components (3a and 4a) may decrease slightly with increasing pressure. The amount of negative shift (2 and 8 cm^{-1}) is too small to conclusively demonstrate mode softening. The remaining components of the doublet (3b and 4) have frequencies that appear nearly linear over the entire pressure range (Fig. 12), but Fermi resonance at high pressure makes it difficult to establish the exact trends, leading to a large uncertainty in the polynomial expansion (Table 5). The frequency of peak 4a appears to have a quadratic dependence on volume. The relative initial slopes of the different bands are consistent among the three olivines studied in that peak 2 has the highest slope and peak 1 has the lowest slope [except for the two peaks (3a and 4a) in fayalite that have frequencies largely independent of volume]. The parallel trends of peaks 4 and 5 of fayalite are consistent with these same peaks not splitting with pressure for forsterite (compare Figs. 8 and 9).

Quantitative analysis of peak positions: Mid-IR bands

The relations of frequency to pressure and volume for the mid-IR modes differ significantly from those of the far-IR bands. Dietrich and Arndt (1982) reported that the frequencies of seven mid-IR bands of Fo$_{84}$ shift linearly with pressure up to the 50-kbar limit of their measurements. Xu et al. (1983) reported that the frequencies of the three most intense bands in synthetic forsterite and fayalite depend linearly on pressure over the 300-kbar range of these experiments. The present data and a complete analysis of the data of Xu et al. (1983) are compiled in Appendix Tables 5 to 7.

All forsterite bands fit linear trends of frequency with pressure (Fig. 10; Table 4). The trends established by Xu et al. (1983) are essentially parallel to the present trends, but shifted to slightly higher frequency. The shift is likely caused by bias in visual removal of the interference fringes. The curvature of ν(16a) with pressure previously observed (Fig. 10) was not detected in the present experiments. The curvature is attributed to proximity of the peak position to the cutoff at 600 cm^{-1} and to the obstructing effect of the interference fringes. Peak 16a pos-
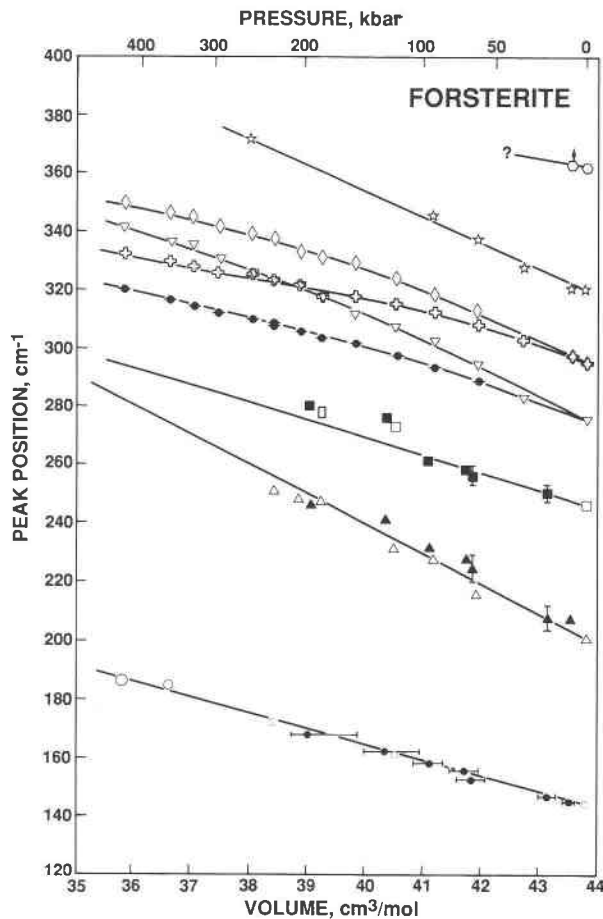
Fig. 11. Far-IR peak positions of forsterite as a function of volume. Symbols are listed in Fig. 8. Filled symbols are for nonhydrostatic single-crystal experiments. Open symbols are for hydrostatic powder experiments. Error bars for volume are shown only for the lowest-energy peak and were calculated from the uncertainties in the pressure determination. The frequencies of all peaks are linearly dependent on volume for pressures below 150 kbar. For the three bands lowest in energy, the linear dependence of ν on volume extends over the entire range of measurements ($P < 425$ kbar). The fit of ν with volume at low compressions is better than the fit of ν with pressure.
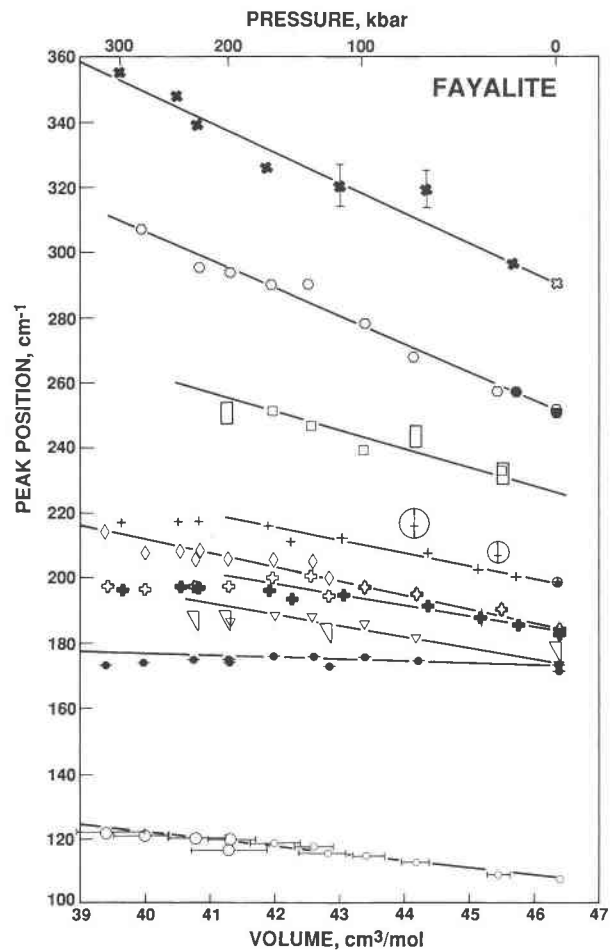
Fig. 12. Far-IR peak positions of fayalite as a function of volume. Symbols are listed in Fig. 8. Filled symbols are for powder experiments. Open symbols are for single-crystal experiments. Error bars for volume are shown for the lowest-energy peak and were computed from the uncertainties in the pressure determination. The frequencies of the three highest-energy peaks and possibly the lowest-energy peak all depend linearly on volume for all pressures measured. The middle-energy peaks (and possibly the lowest-energy peak) show frequencies lower than the extrapolated linear trend at pressures >200 kbar ($V < 41.4$ cm^3/mol).

sibly exhibits a slight departure from constant $d\nu/dP$ at high pressures in that the frequency measured at the highest pressure attained is slightly higher than the linear trend at lower pressures (Fig. 10), but this did not influence the polynomial expansion (Table 4). Peak 16b at 698 cm^{-1} exhibits linear behavior only at pressures above 125 kbar. Below this pressure, the peak position cannot be measured accurately because strong absorptions due to CO_2 gas remaining after purging obliterate this band, or because peak 16b only occurs at high pressure.

The frequencies of all of the mid-IR peaks in forsterite can also be linearly correlated with volume (Fig. 13; Table 5). The trend of peak 16b is reliable only at high pressures, as discussed above. Some curvature is suggest-

ed for peak 16a (Fig. 13), but because its determination depends strongly on the last point, the quadratic analysis of the data cannot be trusted, so that the linear representation of Table 5 was used.

The mid-IR peak positions of fayalite also depend linearly on both pressure (Xu et al., 1983) and volume (Fig. 14), with the possible exception of the combination of peaks 15 and 16a. This band follows two distinct linear trends of ν with V at high and low pressures such that $d\nu/dV$ is larger at higher pressure. The change in $d\nu/dV$ may be attributed to the appearance of a strong band at ~175 kbar (peak 16c) that overlaps with peak 16a and that increases in intensity as pressure increases. Hence, the true peak position may be less than that measured. Un-
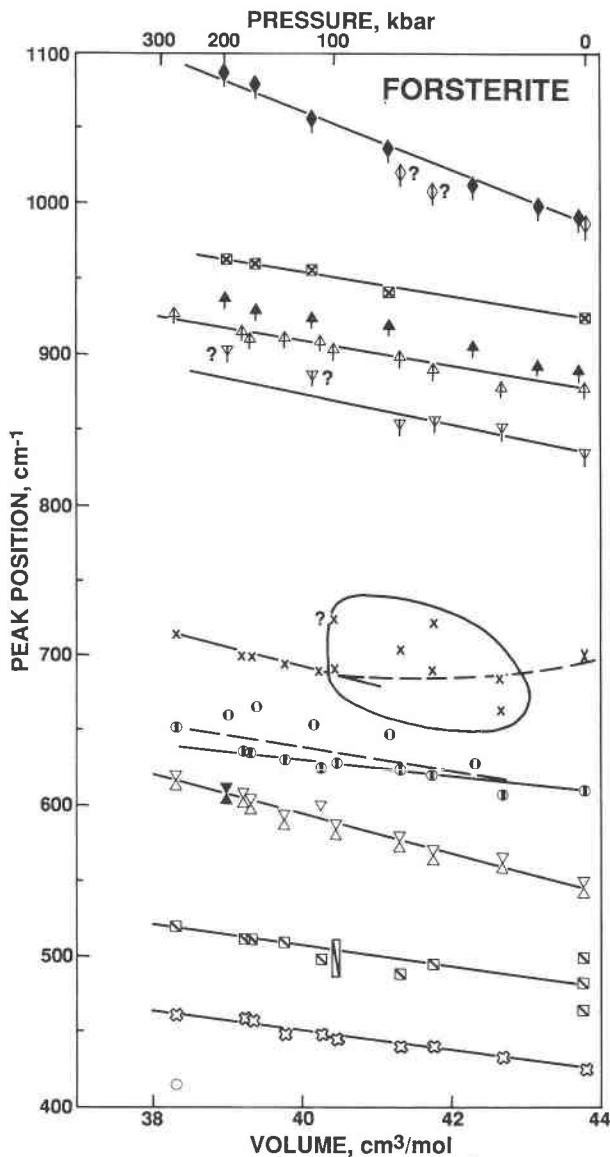
Fig. 13. Dependence of mid-IR peak positions of forsterite on volume. Symbols are listed in Fig. 8. Dots are for overtones (at ~1000 cm⁻¹) or for peaks possibly derived from the β or γ phase. Open symbols are from this work. Closed symbols represent data of Xu et al. (1983). Circled area indicates where the position of peak 16b was difficult to measure accurately because of masking by a strong CO_2 band. All peak positions depend linearly on pressure except for this peak.
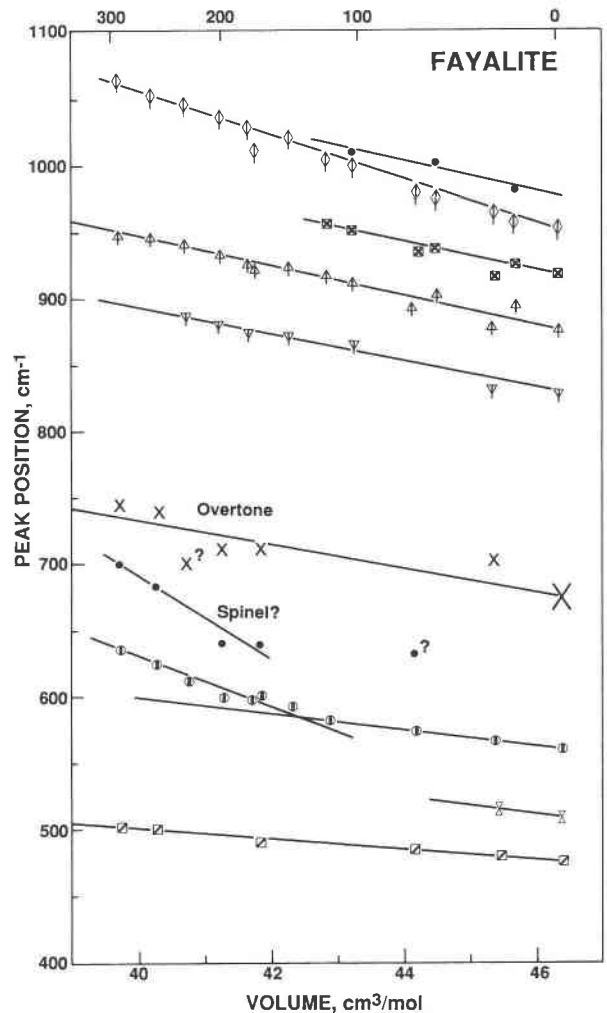

Fig. 14. Volume dependence of mid-IR fayalite data of Xu et al. (1983). All peaks except 16a follow linear trends of frequency with volume. The departure of $\nu(V)$ from the linear trend at low pressures for peak 16a may be due to the growth of a strong band at slightly higher frequency band (16c, ●) at pressures above 170 kbar. This same peak also perturbs the position of peak 16b (×), mostly owing to the low intensity of this band. Symbols are listed in Fig. 8.

Comparison of mid- and far-IR trends

The linear behavior of mid-IR frequencies with pressure (Fig. 10) contrasts with the distinct curvature seen for the far-IR bands (Figs. 8, 9; App. Fig. 3) and may be attributed to the relative incompressibility of the Si tetrahedra as compared to Mg-Fe octahedra (Hazen and Finger, 1982) in that the modes with frequencies above 460 cm⁻¹ have been assigned to Si–O stretching and bending modes, whereas the low-energy modes are connected with translations of the cations and rotations of the SiO₄ groups (Hofmeister, 1987). This suggests that the vibrational modes of the SiO₄ tetrahedra present in the mid-IR are relatively incompressible. The contrasting behavior of the

fortunately, these data could not be deconvoluted because they were erased by a power failure. If peak 16a behaves the same with pressure for fayalite as occurs for forsterite, then the linear trend of ν with volume should hold up to the 300-kbar limit attained by Xu et al. (1983). In subsequent analyses, we will discuss both linear and nonlinear behavior for peak 16a.

far-IR bands (M–O vibrations) in olivine (ν is a linear function of V but not of P) suggests that the crystal compressibility is mainly a function of the octahedral compression, whereas the compression of the tetrahedra is mainly independent of crystal compression. This result agrees with the polyhedral model proposed by Hazen and Finger (1982) based on X-ray determinations of crystal structure at pressure and subsequent high-pressure studies of olivine by Kudoh and Takéuchi (1985) and Kudoh and Takeda (1986).

Pressure and volume derivatives of frequency

The pressure and volume derivatives of the frequency are of interest because these are related to the mode Grüneisen parameters (discussed below). These derivatives were calculated using linear-regression analysis. The pressure derivative $d\nu/dP$ generally increases as frequency increases (Table 4). For the far-IR bands, $d\nu/dp$ of forsterite is almost always higher than $d\nu/dp$ of fayalite, possibly because forsterite frequencies are higher than those of fayalite for far-IR bands (Tables 1 and 4). In contrast, $d\nu/dP$ for the mid-IR bands is approximately independent of Fe content and equal to 0.2–0.4 cm^{-1}/kbar for ν_4, ν_1, and ν_3, whereas $d\nu_2/dP$ is half this value (Table 4) and thus closer to the initial slopes of the far-IR peaks. Mid-IR spectra of forsterite presented here have slopes that are similar to but slightly less than those measured by Xu et al. (1983). For the strong peaks (nos. 12 and 18), our data are the same as those of Fo$_{84}$ by Dietrich and Arndt (1982). For the weaker peaks, two slopes measured are smaller (nos. 17 and 20), and two are larger (nos. 16 and 19, Table 4). The discrepancy can be explained by three factors. (1) Dietrich and Arndt's (1982) data were taken over a much smaller pressure range (50 kbar instead of 250) and therefore have a less well established slope. Moreover, their pressure calibration relies on the reproducibility of spring length. (2) The position of the shoulders may have been determined by different methods; hence the high-low pairing (19—20; 16—17). (3) Intermediate olivines can have a different vibrational character than end-members because of two-mode behavior. Volume derivatives (Table 5) follow similar trends with frequency. For the thermodynamic analysis in preparation, the best-defined bands from each data set will be used, as listed in Tables 4 and 5.

Dependence of width, intensity, and area on volume

The other peak parameters full width at half height (W), intensity (I), and area (the product of width and intensity) are less well defined than frequency. The relatively large uncertainty (even in the hydrostatic runs) results from the large width of the peaks, sloping baselines, and the low resolution used in the far-IR (4 cm^{-1}) to compensate for noise. Thus, whether width, intensity, and area are more closely related to pressure or to volume cannot be determined. An analysis in terms of volume is presented because the frequency of the far-IR bands depends linearly on volume, and because the frequency of the mid-IR bands can be related to either volume or pressure.

Widths of all far-IR peaks except one follow linear trends with volume (Fig. 15; App. Fig. 6), such that most of the peaks have widths that increase gradually as volume decreases. Doublets are an apparent exception: before the two components are resolved, the width increases dramatically as volume decreases (App. Fig. 6, peak 4a). After separation, the width of each component follows a trend similar to those of the other singlets. Widths determined from the present mid-IR forsterite data for peaks 16a and 19 show little or no increase as pressure increases, although the determination has significant uncertainty because of the presence of overlapping bands. Mid-IR widths for fayalite spectra generally increase as volume decreases at a much faster rate than do far-IR widths (App. Fig. 6, top), although the percentage is smaller. A large amount of scatter exists in the mid-IR data because the shoulders on the two intense peaks (18 and 20) interfere in measuring their width and because low intensities of the other peaks make accurate measurement of width difficult. Peak 11 is well-resolved and reasonably intense and shows a width that increases monotonically as pressure increases.

Intensity was rendered independent of sample thinning by examining the change in absorbance of the peaks as the sample was decompressed. During decompression (Fig. 5; App. Fig. 7), the intensities of most peaks increase
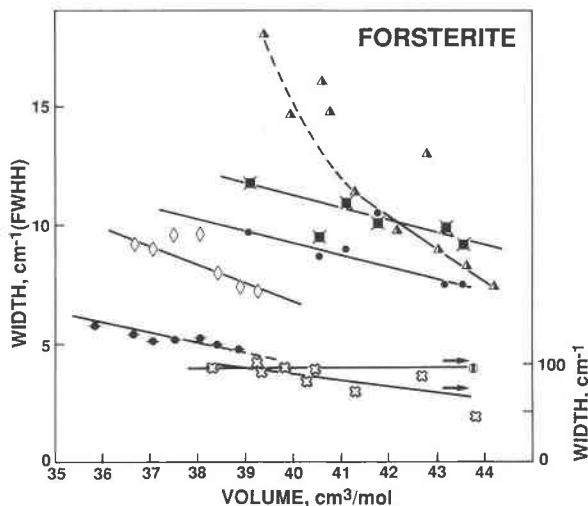

Fig. 15. Dependence of the peak widths of magnesian olivines on volume. The scale for widths for peaks 12 and 16a is at the left. Open symbols, hydrostatic runs on forsterite. Filled symbols, nonhydrostatic forsterite experiments. Half-filled symbols, natural olivine (Fo$_{84}$). Correspondence of peaks with symbols is listed in Fig. 8. Except for peak 2 ($\triangle$) whose width increases dramatically with pressure, all peak widths increase slowly as pressure is increased. Peak width for peak 16a was approximately constant as indicated by the line and one symbol.
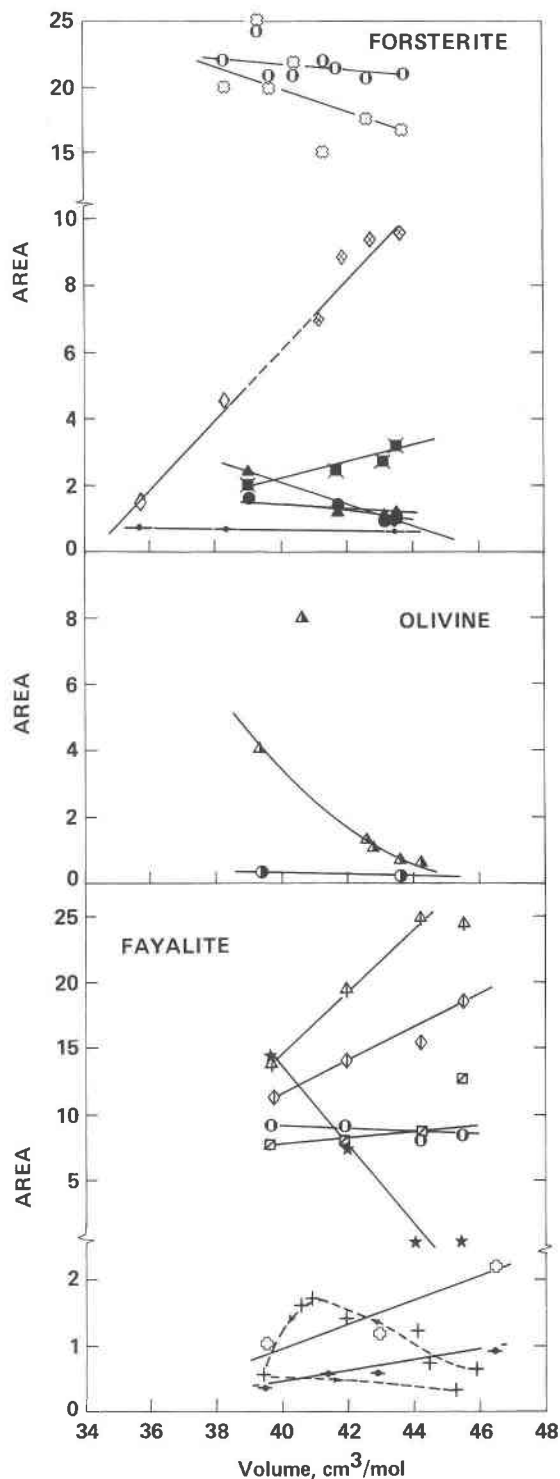
Fig. 16. Peak area as a function of volume during decompression of the sample. (Top) Synthetic forsterite. The area of the irresolvable doublet 4 with X (diamond) was divided in half to facilitate comparison with data on one component at high pressure. (Middle) Natural olivine. (Bottom) Fayalite. Symbols are listed in Fig. 8. Fayalite data indicated by + was collected on compression. The area during decompression was too low for accurate measurement. The effect of thinning is most apparent

(3c, 4b, 2b, 18, 20, 11, 16, 7b). One exception is peak 2 in the magnesian olivine, for which the intensity decreases as pressure decreases. Peaks 1, 5, 9, and 16a remain approximately constant in intensity within a large experimental uncertainty. Mid-IR peaks of fayalite appear to linearly decrease in intensity with volume for data taken during decompression (App. Fig. 7). The uncertainty is large because the shoulders can move at different rates than the main peaks do.

The change of the area (integrated intensity) under the peak with pressure is fundamental, because it is related to the number of atoms involved in the vibration. A more exact analysis is not called for because area measurements are not available for all peaks. Unless the crystal is undergoing a phase transition, peak area is expected to be independent of pressure after thinning effects are removed. During a phase transition, those vibrations that are not present in the new structure should decrease in area as the transition is approached and should disappear as the crystal structure converts to the higher-pressure polymorph; over the same pressure range, bands of the higher-pressure polymorph should appear abruptly and grow. For olivine, all three types of behavior are seen during the decompression experiments, such that the changes are gradual. The areas of peaks 1 and 3ac in forsterite and Fo_{87} are nearly independent of pressure (Fig. 16). Peaks 2b in Fo_{100} and peaks 3c and 11 in fayalite decrease weakly in area as pressure increases. Peaks 4a, 18, and 20 in fayalite and 4b in forsterite sharply decrease in intensity. A slight but definite increase in area as pressure increases was observed for peaks 16a (ν_4) in forsterite and fayalite and 9 (T or R) in forsterite. A definite and strong increase in the area with pressure was noted for two peaks: peak 2a in the magnesian olivines and peak 16c in fayalite (Fig. 16). Note that the different behaviors of peaks 3c and 4b in forsterite occurred during the same hydrostatic experiment.

CALCULATION OF MODE GRÜNEISEN PARAMETERS

Calculation of the first and second mode Grüneisen parameters (γ_i and q_i) from frequency and pressure determinations is analogous to deriving bulk modulus K_T solely from volume and pressure measurements. Bulk modulus is difficult to calculate because its initial value $K_T(0)$ depends on the value chosen for its pressure derivative K', and for most minerals of geophysical interest, the volume does not exhibit strong curvature with pres-

←

between the three lowest-volume points ($P > 350$ kbar), but probably also occurred during compression at low pressure. Thus, the actual increase in area with volume for peak 4 in fayalite is larger than that depicted. Increases in area are definitely observed for peak 2a in magnesian olivine and for a new band (star) near 700 cm^{-1} in fayalite mid-IR. Two peaks show slight increases in area (1 and 16) that are within the experimental uncertainties. All other peaks have areas that decrease or remain constant as volume decreases (pressure increases).

sure. For bulk-modulus determinations, the dilemma is resolved by direct measurement of $K_T(0)$ by ultrasonic or Brillouin scattering techniques. Unfortunately, the first mode Grüneisen parameter cannot be independently calculated at this time. However, the strong curvature in $\nu(P)$ and $\nu(V)$ for several far-IR bands allows reasonably accurate calculation of their Grüneisen parameters. For the remaining bands, we will show how a range of γ_i and q_i can be ascertained from several equivalent formulations.

The first mode Grüneisen parameter is defined as

$$\gamma_i = -d \ln \nu_i / d \ln V, \tag{1a}$$

which is equivalent either to

$$\gamma_i(V) = -(V/\nu_i)(d\nu_i/dV) \tag{1b}$$

or to

$$\gamma_i(P) = (K_T/\nu_i)(d\nu_i/dP). \tag{1c}$$

From Equations 1a–1c it is obvious that uncertainties in the equation of state (EOS) will strongly affect determination of γ_i. Fortunately, $K_T(0)$ is accurately known for forsterite and fayalite, so that the uncertainty in the EOS is contained in K_0' (ca. $\pm 8\%$, see Graham et al., 1988; and earlier discussion). $K'(P)$ is assumed to be constant, but this is probably not true (Bassett et al., 1982). Given the absence of values for the second derivative q_i for other substances (and, as we shall demonstrate, assumption of integer values such as 0, 1, or 2 is not justified), the approach least prone to prejudices and errors is to apply Equations 1a–1c to the appropriate polynomial representations of the data listed in Tables 4 and 5. Each formulation has an associated *precision*. By comparing the three results, an average γ_i with an estimate of its *accuracy* can be ascertained. The second Grüneisen parameter is then calculated in a consistent manner from the three equivalent formulas. By definition,

$$q_i = d \ln \gamma_i / d \ln V. \tag{2a}$$

Equivalently,

$$q_i = (V/\gamma_i)(d\gamma_i/dV) = 1 + \gamma_i - (V^2/\gamma_i\nu_i)(d^2\nu_i/dV^2) \tag{2b}$$

$$q_i = -(K_T/\gamma_i)(d\gamma_i/dP) = \gamma_i - K' - (K_T^2/\gamma_i\nu_i)(d^2\nu_i/dP^2). \tag{2c}$$

It may be argued that the polynomial expansions are not true representations of data and that some other function may be more appropriate. We shall show this is inconsequential compared to the uncertainty in the calculation resulting from the dependence of the first Grüneisen parameter upon the second and vice versa.

Calculation of γ_i and q_i from $\nu(P)$

Application of Equations 1c and 2c to the polynomial expansions of Table 4 gives $\gamma_i(0)$ values ranging from 0.1 to 1.9 for forsterite and 0.1 to 1.7 for fayalite and $q_i(0)$ values from -5 to 26 (Table 6). The precision in γ_i of roughly $\pm 10\%$ stems from those in the polynomial coefficients of expansion, whereas the lesser precision in q_i of

± 0.6 comes from that of K'. The large negative values of q of about -4.5 are a direct consequence of the linear dependence of frequency on pressure for many of the bands (Figs. 8, 9, 10; Table 4). In this case, Equation 2c reduces to

$$q_i = \gamma_i - K'. \tag{3}$$

The value of q_i obtained from Equation 3 is the minimum allowed, because any curvature of frequency with volume will increase q_i (Eq. 2c). Positive or slightly negative values of q_i from -2 to $+26$ occur for the bands showing distinct curvature of frequency with pressure.

Calculation of γ_i and q_i from $\nu(V)$

Application of Equations 1b and 2b to the polynomial representations of Table 5 gives $\gamma_i(0)$ values ranging from 0.13 to 2.0 for forsterite and 0.09 to 1.6 for fayalite and a bimodal distribution of $q_i(0)$ values from 1.1 to 13 (Table 6). The precision in γ_i of roughly $\pm 10\%$ stems from that of the polynomial coefficients of expansion, whereas the lesser precision in q_i of ± 0.6 results from the above and that of K'. The low q_i values of 1.1 to 3.0 occurring for the majority of the bands are a consequence of the linear dependence of frequency on volume (Figs. 12 to 14). For this case, Equation 2b reduces to

$$q_i = 1 + \gamma_i. \tag{4}$$

Thus, the value of q_i decreases slightly as pressure increases, because γ_i decreases as P increases. It is important to note that q cannot be larger than 3 or curvature would show in analysis of frequency as a function of volume. Thus, although Equation 4 does not represent the maximum, because $d^2\nu/dV^2$ can be either positive or negative, the values of about 2 derived from it are close to the maximum possible.

For the doublets 3 and 4 in forsterite and peaks 1, 3, 4, 5, and 16 in fayalite, γ_i was calculated as a function of volume (Table 7) from Equation 1b using the fits of $\nu(V)$ derived from linear-regression analyses (Table 7). Except for peak 16 (ν_4 in fayalite), γ_i decreases as pressure increases (Fig. 14; Table 7), but this trend may not be appropriate to olivine, as discussed later. For the peaks with strong curvature, γ_i decreases by 75% whereas for peaks with linear dependence of ν on V, γ_i decreases by 30%. Peaks with quadratic representations yield moderate $q_i(0)$ values of 5 to 7 that are nearly independent of pressure whereas those with cubic expansions have large $q_i(0)$ of 10 to 13 that decrease rapidly as pressure increases (Table 7).

Calculation of γ_i and q_i from logarithmic expansions

The data $[\ln \nu(\ln V)]$ were fit to polynomials of orders 2 to 5 through a linear-regression analysis. This approach does not assume that $q_i(0)$ is zero, although one result is that $q_i(0)$ is zero for the linearly dependent peaks. For all cases, $\ln \nu_i$ depends linearly on $\ln V$ at pressures below about 120 kbar (Figs. 17, 18; App. Fig. 8), which is approximately the stability limit of magnesian olivine. Ex-

TABLE 6. First and second mode Grüneisen parameters of infrared bands in olivine

Peak	ν_0	$\gamma_i(0) =$ $(K_T/\nu_0)(d\nu/dP)$	$q_i(0)$ (Eq. 2c)	$\gamma_i(0) =$ $(-V_0/\nu_0)$ $(d\nu/dV)$	$q_i(0)$ (Eq. 2b)	$\gamma_i =$ $(-d \ln \nu)/$ $(d \ln V)$	γ_i at high P	$\gamma_i(0)$ Preferred	$q_i(0)$ Preferred
Forsterite (hydrostatic)									
1	142	1.40 ± 0.02	−1.3	1.65 ± 0.03	2.65	1.31 ± 0.05		1.52 ± 0.12	0.7 ± 2
2	201	1.85 ± 0.02	−0.3	1.98 ± 0.11	2.98	1.64 ± 0.09		1.91 ± 0.08	1.4 ± 1.6
3c	275	1.22 ± 0.05	3.2	1.52 ± 0.10	10.1	1.06 ± 0.06 ($P < 120$)	0.57 ± 0.01 ($P > 200$)	1.37 ± 0.20	6 ± 4
3b	275	1.66 ± 0.08	2.9	1.71 ± 0.10	5.1	1.46 ± 0.07 ($P < 120$)	0.85 ± 0.04 ($P > 150$)	1.69 ± 0.11	4.0 ± 1.1
4ac	295	1.10 ± 0.05	4.7	1.34 ± 0.10	12.7	0.88 ± 0.04 ($P < 120$)	0.42 ± 0.03 ($P > 150$)	1.25 ± 0.15	8.7 ± 4
4b + 5 + 6	295	1.42 ± 0.05	3.3	1.52 ± 0.13	6.2	1.22 ± 0.04 ($P < 100$)	0.59 ± 0.03 ($P > 200$)	1.47 ± 0.10	4.8 ± 1.4
7	320	1.20 ± 0.07	−0.6	1.26 ± 0.27	2.3	1.07 ± 0.05		1.23 ± 0.10	0.9 ± 1.4
8	362	0.71 ± 0.04	−4.3	1.04 ± 0.10	2.04	1.00 ± 0.10		0.85 ± 0.20	−1.2 ± 2.2
Forsterite (nonhydrostatic)									
2b	246	0.96 ± 0.07	−4.0	1.12 ± 0.10	2.18	1.00 ± 0.06		1.04 ± 0.1	−1.0 ± 3
9	421	0.94 ± 0.02	−4.5	0.80 ± 0.06	1.80	0.72 ± 0.06		0.65 ± 0.20	−1.4 ± 3
10c + 11	474	0.38 ± 0.03	−4.6	0.77 ± 0.07	1.7	0.69 ± 0.08		0.58 ± 0.20	−1.5 ± 3
14 + 15	545	0.75 ± 0.05	−4.3	1.01 ± 0.05	2.0	0.90 ± 0.05		0.88 ± 0.18	−1.2 ± 3
16a	609	0.28 ± 0.03	−4.7	0.50 ± 0.05	1.5	0.46 ± 0.05		0.39 ± 0.13	−1.6 ± 3
16b	698	0.11 ± 0.01	−4.9	0.13 ± 0.01	1.1	0.12 ± 0.10		0.12 ± 0.03	−1.9 ± 3
17	837	0.47 ± 0.05	−4.5	0.41 ± 0.08	1.4	0.40 ± 0.10		0.44 ± 0.07	−1.6 ± 3
18	876	0.32 ± 0.03	−4.7	0.46 ± 0.03	1.5	0.40 ± 0.03		0.39 ± 0.10	−1.6 ± 3
19	925	0.23 ± 0.02	−4.8	0.37 ± 0.03	1.4	0.38 ± 0.03		0.30 ± 0.09	−1.7 ± 3
20	986	0.68 ± 0.07	−4.3	0.90 ± 0.05	1.9	0.81 ± 0.02		0.79 ± 0.18	−1.5 ± 3
Fo$_{87}$ (nonhydrostatic)									
1	138	2.30 ± 0.35	1.2	1.44 ± 0.15	2.4	1.25 ± 0.12		1.90 ± 0.50	1.8 ± 1.6
2a	198	3.08 ± 0.32	1.3	2.36 ± 0.20	3.36	1.98 ± 0.12		2.70 ± 0.30	1.6 ± 1.3
2b	242	2.49 ± 0.25	8.4	0.92 ± 0.09	1.92	0.82 ± 0.10		1.70 ± 0.70	4.5 ± 4.5
Fayalite (nonhydrostatic)									
1	107.5	0.91 ± 0.09	26.5	1.37 ± 0.30	6.5	0.90 ± 0.10	0.3 ($P > 200$)	1.14 ± 0.24	ca. 6
3ac	173	0.11 ± 0.40	−5.1	0.09 ± 0.03	1.1	0.18 ± 0.04	0.17 ($P > 150$)	0.10 ± 0.02	−2.0 ± 3.0
3b	173	1.22 ± 0.07	3.3	0.71 ± 0.07	1.7	0.94 ± 0.07		0.96 ± 0.25	2.5 ± 1.2
4ac	183.1	0.92 ± 0.07	1.8	1.41 ± 0.02	11.3	0.73 ± 0.10	0.0 ($P > 200$)	1.16 ± 0.25	6.5 ± 5
4b	183.4	1.38 ± 0.08	1.27	0.96 ± 0.10	2.0	1.10 ± 0.10	0.5 ($P > 150$)	1.17 ± 0.20	1.6 ± 0.3
5	197.5	1.02 ± 0.06	0.90	1.28 ± 0.05	8.2	0.80 ± 0.10	~0 ($P > 250$)?	1.15 ± 0.10	4.5 ± 3.5
6	230	0.65 ± 0.06	−4.6	0.91 ± 0.10	1.9	0.88 ± 0.08		0.78 ± 0.13	−1.4 ± 3.5
8	252	0.99 ± 0.10	−4.2	1.59 ± 0.07	2.6	1.30 ± 0.05		1.30 ± 0.30	−0.8 ± 3.5
9	290	0.93 ± 0.30	−4.3	1.45 ± 0.15	2.4	1.35 ± 0.01		1.20 ± 0.30	−0.9 ± 3.5
11 + 12?	477	0.27 ± 0.02	−5.0	0.36 ± 0.03	1.4	0.31 ± 0.02		0.31 ± 0.05	−1.8 ± 3.5
13 + 14	507	0.80 ± 0.08	−4.4	0.80 ± 0.08	1.8	0.83 ± 0.06		0.80 ± 0.08	−1.3 ± 3.5
15 + 16	557	0.49 ± 0.05	−4.7	0.73 ± 0.07	1.7	0.64 ± 0.03	1.3* ($P > 150$)	0.60 ± 0.13	−1.5 ± 3.5
17	827	0.40 ± 0.06	−4.8	0.60 ± 0.04	1.6	0.57 ± 0.03		0.50 ± 0.10	−1.6 ± 3.5
18	875	0.36 ± 0.06	−4.9	0.60 ± 0.04	1.6	0.54 ± 0.03		0.48 ± 0.12	−1.6 ± 3.5
19	916	0.34 ± 0.08	−4.9	0.62 ± 0.04	1.6	0.58 ± 0.09		0.48 ± 0.14	−1.6 ± 3.5
20	950	0.57 ± 0.02	−4.7	0.87 ± 0.03	1.9	0.75 ± 0.03		0.72 ± 0.15	−1.4 ± 3.5

Note: The $q_i(0)$ values from Eqs. 2b and 2c are uncertain by ± 0.6, and $q_i(0)$ of Eq. 2a is approximately zero.
* The trend at high pressure may be influenced by the appearance of a new peak at high pressure.

cept for peaks 1 and 16a in fayalite and the doublets (peaks 3 and 4), linear trends of ln ν vs. ln V exist over the entire range of measurements. At high pressure, either ln ν of peaks 1 and 16a in fayalite is constant or all of the doublets follow a different linear trend of ln ν with ln V at high compared to that at low pressure (Figs. 17 and 18). Above 150 kbar, ln ν of peak 16a in fayalite may rise more steeply with ln V than it does at low pressure, in contrast to the behavior of the far-IR bands. The data could not be fit adequately to a low-order polynomial ($M < 5$), suggesting that the straight line fits over the "low"

and "high" pressure regimes may be an accurate representation of the data. It is possible that the samples are undergoing a phase transition (discussed later).

The $\gamma_i(0)$ values range from 0.1 to 1.6 for forsterite and 0.1 to 1.4 for fayalite (Table 6). The linear dependence of ln ν on ln V (Figs. 17, 18; App. Fig. 8) suggests that the second mode Grüneisen parameter q_i is close to zero for most modes up to 400 kbar. For the doublets (3, 4) in forsterite and peaks 1, 3, 4, 5, 6, and 16 in fayalite, plots of ln γ_i vs. ln V (Figs. 19, 20), show that q_i ranges from zero to infinity, such that at 1 atm $q_i(0)$ ranges from
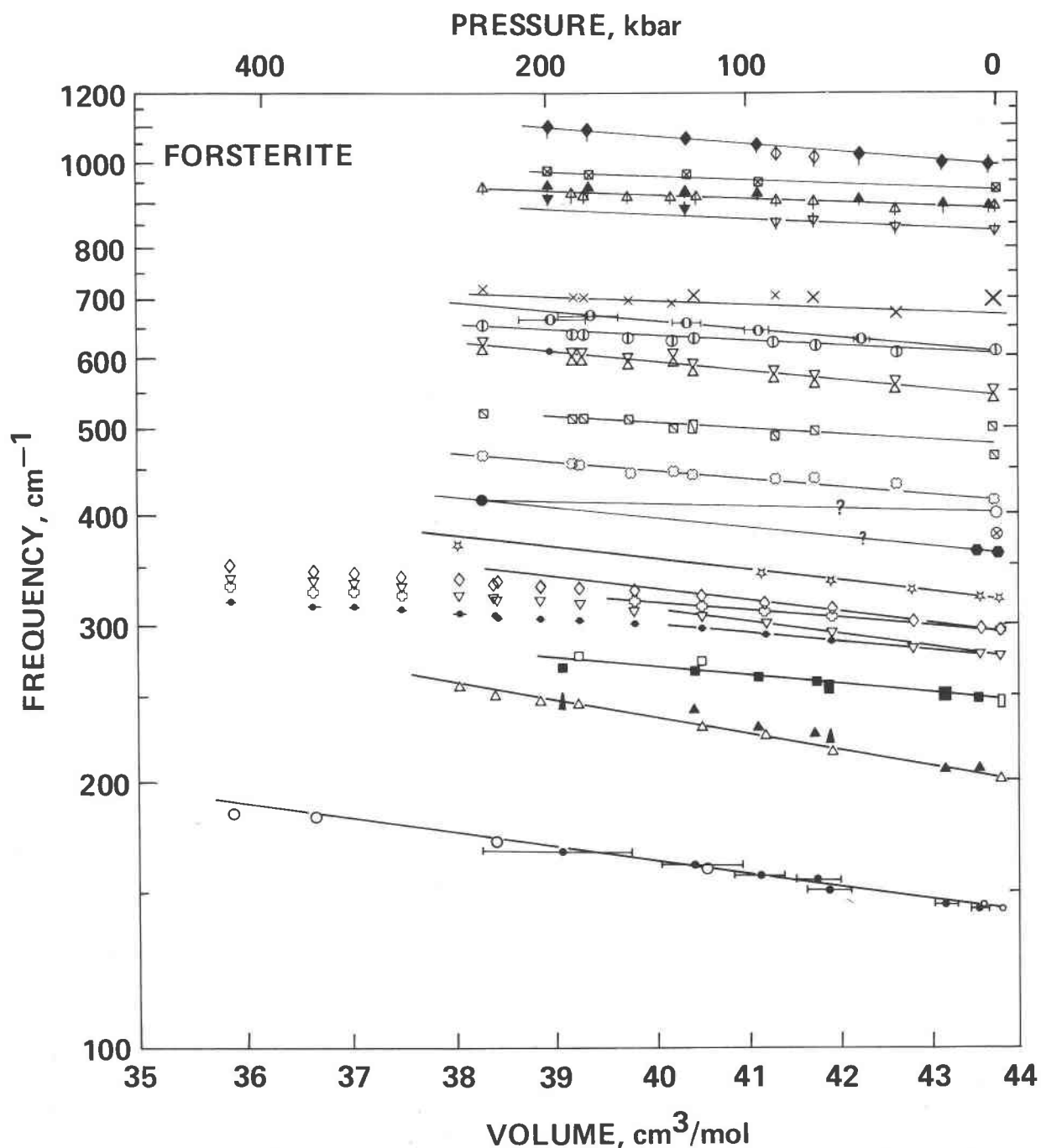
Fig. 17. Log-log plot of band positions of forsterite vs. volume. Symbols are listed in Fig. 8. Uncertainties in volume are indicated by the error bars on three of the peaks. Mid-IR data ($\nu > 400$ cm^{-1}) of Xu et al. (1983) are shown as filled symbols. All bands except 3 and 4 (the doublets) show linear dependence of $d(\ln \nu)$ on $d(\ln V)$. Far-ID data ($\nu < 400$ cm^{-1}) from nonhydrostatic experiments are indicated by filled symbols.

zero to 12.7 and at pressures above 150 kbar, q_i ranges from zero to infinity. Fayalite IR bands (Fig. 20) show a marked dependence of q on volume, whereas forsterite bands (Fig. 19) show a weak dependence.

To circumnavigate the problem of "averaging" over pressure (as a log-lot plot does), γ_i was calculated for for-

sterite bands and peak 16a in fayalite from the instantaneous derivatives as measured from Figures 11 to 14. This approach was not used for the other fayalite peaks because of the larger amount of scatter and experimental uncertainty associated with this data set. The resulting plot of $\ln \gamma_i$ vs. $\ln V$ (Fig. 19) showed a moderate amount

TABLE 7.	Pressure dependence of the first (γ_i) and second (q_i) mode Grüneisen parameters for selected bands

	P (kbar)									
	0.001	10	25	50	75	100	125	150	200	250
Forsterite										
V	43.79	43.46	42.99	42.25	41.60	40.98	40.42	39.91	38.98	38.15
Instantaneous derivative										
3ac	1.15	1.13	1.10	1.04	0.98	0.88	0.78	0.75	0.67	0.56
3b	1.51	1.49	1.45	1.39	1.34	1.30	1.25	1.21	1.12	1.02
4ac	1.05	1.03	0.92	0.86	0.38	0.63	0.54	0.48	0.43	0.41
4b	1.31	1.28	1.24	1.12	0.99	0.86	0.78	0.75	0.67	0.58
Polynomial fit										
1	1.65	1.61	1.57	1.50	1.44	1.39	1.35	1.30	1.24	1.18
2a	1.98	1.94	1.88	1.79	1.72	1.65	1.59	1.54	1.45	1.38
2b	1.12	1.10	1.08	1.04	1.01	—	0.95	0.93	0.89	0.85
3ac	1.52	1.41	1.27	1.07	0.93	0.82	0.74	0.68	0.60	0.56
	(10.1)	(10.0)	(9.8)	(9.3)	(8.7)	(7.9)	(7.1)	(6.2)	(4.3)	(2.4)
3b	1.71	1.64	1.55	1.42	1.32	1.22	1.14	1.07	0.96	0.86
	(5.15)	(5.10)	(5.10)	(5.0)	(4.96)	(4.93)	(4.91)	(4.91)	(4.93)	(4.96)
4ac	1.35	1.22	1.07	0.86	0.71	0.60	0.52	0.47	0.41	0.39
	(12.7)	(12.7)	(12.6)	(12.3)	(11.7)	(10.7)	(9.5)	(7.7)	(4.0)	(0.17)
4b	1.52	1.45	1.35	1.21	1.10	1.00	0.91	0.83	0.71	0.60
	(6.25)	(6.26)	(6.28)	(6.35)	(6.45)	(6.58)	(6.73)	(6.90)	(7.32)	(7.84)
7	1.25	1.23	1.20	1.16	1.12	1.08	1.06	1.03	0.98	0.94
Fayalite										
V	46.39	46.01	45.53	44.77	44.07	43.12	42.84	42.30	41.35	40.45
Instantaneous derivative										
1	1.16	1.14	1.12	1.08	1.05	0.91	0.77	0.72	0.63	0.47
3ac	0.14	0.13	0.12	0.11	0.10	0.07	0.03	0	−0.06	−0.1
3b	0.74		3	0.67		0.45	0.38	0.2	0.1	0
4ac	0.84	0.83	0.81	0.79	0.73	0.60	0.48	0.36	0.16	0
4b	1.12	1.09	1.07	1.03	1.00	0.97	0.95	0.92	0.88	0.84
5	0.93			0.87		0.74	0.64	0.47	0.22	0
16a	0.53	0.54	0.56	0.67	0.72	0.74	0.80	0.82	0.89	1.01
16b	0.67	0.66	0.65	0.63	0.61	0.60	0.59	−0.9	1.11	1.06
Polynomial fit										
1	1.37	1.30	1.21	1.08	0.96	0.87	0.79	0.71	0.59	0.49
	(6.5)	(6.6)	(6.6)	(6.8)	(7.0)	(7.2)	(7.5)	(7.8)	(8.5)	(9.4)
4a	1.41	1.29	1.13	0.90	0.70	0.53	0.39	0.25	0.03	−0.16
	(11.2)	(11.7)	(12.5)	(14.3)	(17.0)	(20.8)	(27.2)	(39.3)	(326)	(−53)
5	1.28	1.20	1.09	0.93	0.80	0.69	0.59	0.51	0.36	0.24
	(8.2)	(8.4)	(8.7)	(9.2)	(9.9)	(10.7)	(11.7)	(13.0)	(16.7)	(23.3)

Note: The q_i values are in parentheses.

of scatter around straight lines. The slope of the lines (q_i) from the instantaneous derivatives is within the uncertainty ($\sim 20\%$) of the determination of q from polynomial fits of $\nu(V)$ (Table 7). The higher-energy components of both doublets in forsterite (peaks 3 and 4) initially have q values of 5 to 6 and remain at these values to 200 kbar, above which q appears to increase, but this is uncertain because of limits in accuracy of measurement. The lower-energy components of the doublets initially have large q values (10 to 13) that steadily decrease to zero (Table 7). For forsterite, slight differences in q_i result from the two approaches (Fig. 20). For the polynomial fits of $\nu(V)$, the initial and final values of q_i are highest. The closest correspondence to q_i from the instantaneous derivatives occurs at intermediate volumes. We suggest that the final values of q_i from the polynomial fits may be overestimated because of the statistical overweighting of the endpoint frequencies.

In fayalite, stronger curvature in frequency as a function of volume is seen, leading to more rapid changes of the mode Grüneisen parameter γ_i and its derivative q_i with volume. The different behaviors of Mg and Fe olivines can be ascribed to their relative stabilities with pressure: at $\sim 1000\ °C$), forsterite transforms to spinel at 130 kbar, whereas fayalite transforms at 60 kbar. Peak 4c exhibits only a faint curvature of ln ν with ln V (Fig. 20). For this band ln γ_i is linear with ln V, having a slope q of 2. The other far-IR bands initially (below 75 kbar) all have slopes of 0–3. The slopes increase steadily, reaching infinity above 200 kbar for the several bands. Band 3b exhibits mode softening: by 150 kbar, q is infinity. Above 150 kbar, q decreases to 25 (as the frequency decreases from its maximum value). One of the mid-IR bands of fayalite shows behavior that is markedly different from any other band in that γ_i increases as volume decreases (peak 16a, circle with two bars in Fig. 20). The circles with two bars represent polynomial fits of ν with volume. A more accurate representation may be two linear trends of $\nu(V)$ at high and low pressures. This is represented by the circles with one bar in Figure 20. The position of peak 16a may have been influenced by the appearance of a higher energy band at pressures above 100 kbar. If this is the case, then the initial trend of peak 16a is given by the circles with one bar in Figure 20, and it behaves like

TABLE 7.—Continued

P (kbar)			
300	350	400	q_i
Forsterite			
37.40	36.73	36.12	
Instantaneous derivative			
0.52	0.50	0.49	4.5
0.90	0.79	0.68	2.5–9.0
0.36	0.35	0.34	5.9
0.52	0.50	0.49	5.5
Polynomial fit			
1.13	1.09	1.05	$1 + \gamma_i$
1.31	1.26	1.21	$1 + \gamma_i$
0.82	0.80	0.77	$1 + \gamma_i$
0.54	0.55	0.56	variable
(0.6)	(−0.8)	(−1.9)	
0.78	0.71	0.65	5.05 ± 0.15
(5.02)	(5.09)	(5.17)	
0.40	0.43	0.47	variable
(−2.9)	(−5.0)	(−6.1)	
0.51	0.43	0.37	variable
(8.48)	(9.26)	(10.22)	
0.91	0.88	0.85	$1 + \gamma_i$
Fayalite			
39.69			
Instantaneous derivative			
0.33			2.5–13
−0.17			3–28
0			~0–∞
0			1.7–∞
0.82			2.00
0			2–∞
1.08			−2.5−−4.6
1.03			2.6
Polynomial fit			
0.40			6.6
(10.5)			
−0.33			variable
(−25)			
0.132			variable
(38.8)			

fact that both ν and V change only slightly (10–20%) over the range of measurements, (2) the moderate experimental uncertainties derived from the difficulty in determining the positions of broad, weak peaks, and by (3) the fact that γ_i and q_i are interdependent.

The value of $\gamma_i(0)$ calculated by Equation 1c from $d\nu/dP$ is always lower than $\gamma_i(0)$ from $d\nu/dV$ through Equation 1b (Table 6). For the bands exhibiting linear dependence of frequency on pressure and volume (i.e., the rotations and Si-O internal modes), the logarithmic determination of γ_i is in between values based on pressure and volume expansions of the frequency, which is consistent with the values determined for $q_i(0)$ for each approach (Table 6). For the bands exhibiting nonlinear behavior (i.e., the M-O translations), the logarithmic determination of γ_i is lower than $\nu(P)$ and thus $\nu(V)$, and the same generally holds for q_i.

The values of $\gamma_i(0)$ calculated from the three approaches (Eqs. 1a, 1b, and 1c) vary outside of the experimental precision (Table 6). The mode Grüneisen parameter derived from a log–log relation is essentially an average over pressure, whereas γ_i from $d\nu/dV$ or $d\nu/dP$ is probably closer to the initial value. Hence, the most accurate values at 1 atm are likely given by an average of $\gamma(P)$ and $\gamma(V)$, with an uncertainty that spans the values determined from the two approaches. The resultant $\gamma_i(0)$ values are uncertain by roughly ±20% whereas $q_i(0)$ values are uncertain by ±3 (Table 6). The resultant negative values for many of the bands appear suspicious, but as will be shown in a subsequent paper (in prep.) slight negative values are reasonable in that the thermal second Grüneisen parameter determined from heat capacity as a function of pressure is about 1.0 and such a value can only be obtained from averaging q_i if most of the bands have negative q_i because of the very large values of q_i for the doublets.

any of the others. The trend at high pressure is due to interference of the new band with peak 16. The second trend at higher pressures parallels the first and also behaves as do all the other peaks. This behavior is consistent with the higher-pressure peak representing a different mode. For fayalite, all bands under nonhydrostatic compression have initial second mode Grüneisen parameters below three, some of which increase gradually to about 6 at twice the transition pressure of 60 kbar, and thereafter increase rapidly to infinity. Under *hydrostatic* compression, the low q region may be extended to higher pressures (estimated as 150–200 kbar, by analogy to forsterite), and the rapid increase in q_i for fayalite would be raised from 150–200 kbar to 300 to 400 kbar. A rapid increase in q_i for forsterite is inferred to occur above about 600 kbar.

Comparison of the three approaches

The fact that for many bands, linear dependencies were found for all of $\nu(P)$, $\nu(V)$, and $\ln \nu(\ln V)$ appears to be contradictory, but this result can be explained by (1) the

Discussion of the variation in mode Grüneisen parameters

Comparison of the initial mode Grüneisen parameters of forsterite to those of fayalite (Table 6) shows that the Fe content affects the far-IR bands more than the mid-IR bands. This is concordant with assignments of far-IR bands to the metal ions and of mid-IR bands to tetrahedral vibrations of SiO_4. Four of the mid-IR bands (ν_4, ν_1, and $2\nu_3$) have $\gamma_i(0)$ values that are approximately the same (±10%) for forsterite and fayalite. The remaining symmetric stretching band ν_2 has a higher $\gamma_i(0)$ for forsterite, but for this same band in Fo_{84} has a value equal to that of fayalite (Table 6). The value (0.38) of $\gamma_i(0)$ for $\lambda(19)$ in forsterite (ν_3) may be low because the position of a shoulder is imprecise.

Among the far-IR bands, substitution of Fe for Mg exerts a strong to moderate influence on $\gamma_i(0)$, depending on the band. For bands 1 and 4ab, $\gamma_i(0)$ of the end-members is the same within 10%. For bands 3ab, $\gamma_i(0)$ of forsterite is 2 to 15 times larger, whereas for bands 8 and 9, $\gamma_i(0)$ of forsterite is roughly one half that of fayalite. The variation is due to a combination of large differences in
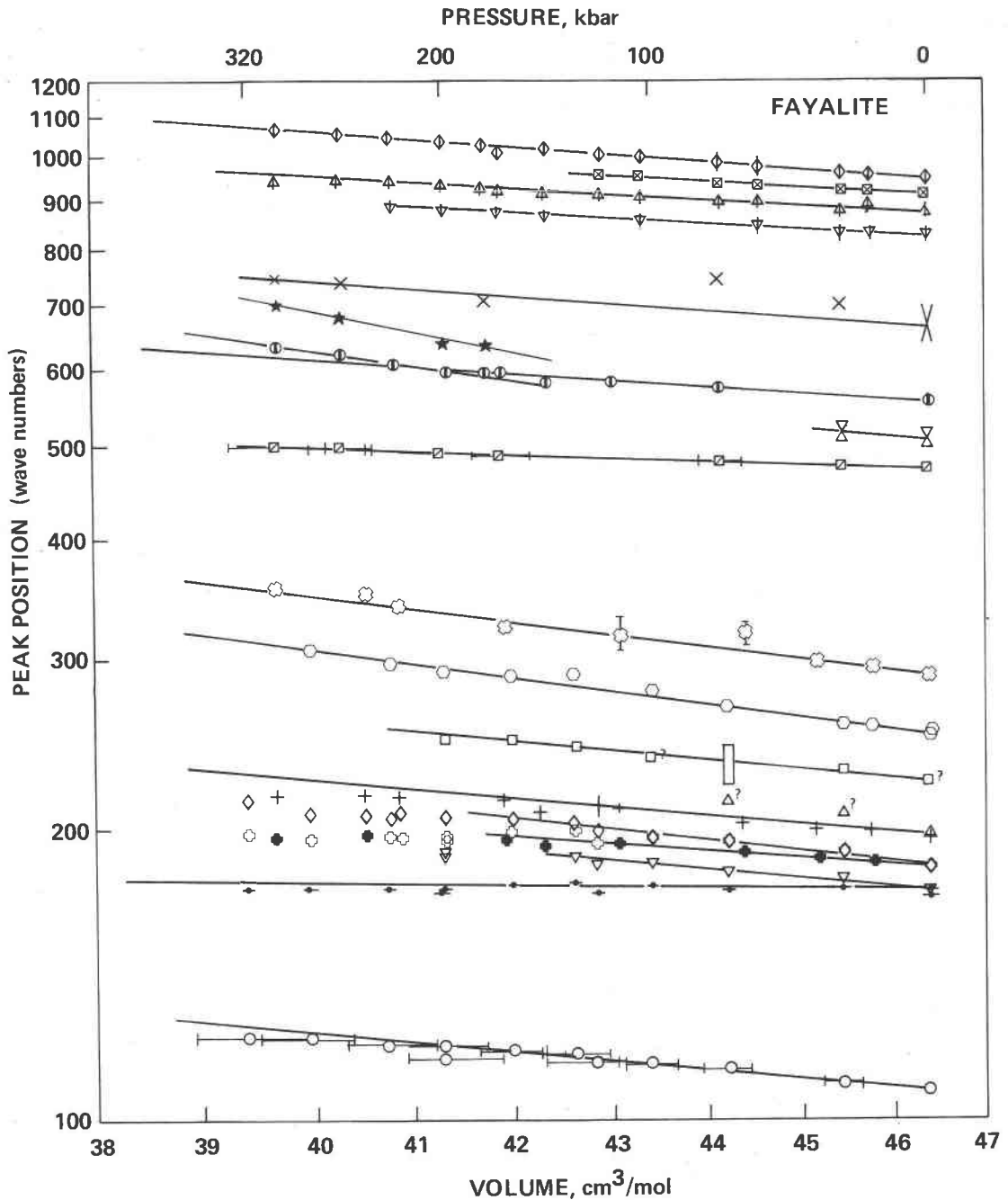
Fig. 18.   Log–log plot of band positions vs. volume for fayalite. Symbols are listed in Fig. 8. The mid-IR data of Xu et al. (1983) are included. All peaks except 3, 4, 5, 16, and possibly 1 show linear dependence of ln ν on ln V.

relative initial frequencies between forsterite and fayalite and small changes in the slopes (Table 6). The band positions relate directly to the assignment: shifts in frequency from forsterite to fayalite decrease in order of M-ion translations, rotations, SiO_4 translations, and SiO_4 internal modes (Hofmeister, 1987). Therefore, in estimating $\gamma_i(0)$ for bands missing from fayalite spectra for a future paper (in prep.), $d\nu/dV$ will be used for the analogous band in forsterite and vice versa; $\gamma_i(0)$ will not be used

directly. For the mid-IR bands, where the frequency difference is small and $d\nu/dV$ varies little, $\gamma_i(0)$ is the same for analogous bands (Table 6).

The most striking difference in $\gamma_i(0)$ occurs between the far-IR and the mid-IR bands. The far-IR bands cover a larger range of $\gamma_i(0)$ (from 0.0 to 2.52) whereas $\gamma_i(0)$ of the mid-IR bands only ranges from 0.32 to 1.0. The values of $\gamma_i(0)$ are generally higher for the far-IR bands: all except one of the far-IR bands have $\gamma_i(0)$ of greater than
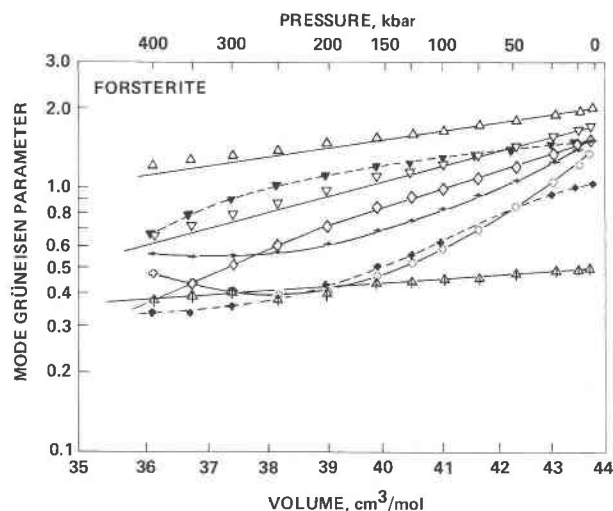
Fig. 19. Plot of ln γ_i vs. ln V used to determine q_i for forsterite. Symbols are listed in Fig. 8. Open symbols, γ_i calculated from polynomial fits for $\nu(V)$ (App. Table 5). Linear dependencies of ν on V yield nearly constant q of $1 + \gamma_i(0)$. The increase in q for the open cross at very high pressure is suspect because of the uncertainty of $\nu(P)$ at the end of the data collection and the cubic dependence on $\nu(V)$. Filled symbols, $\gamma_i(V)$ calculated from the instantaneous derivative $(d\nu/dV)$. The S-shaped curve indicates two different linear trends of frequency with volume at high and low pressures.

Fig. 20. Plot of ln γ_i vs. ln V used to estimate q_i for fayalite. Peak symbols are listed in Fig. 8. Some points are omitted for clairity. Open symbols are for γ_i calculated from polynomial fits of ν as a function of V. Solid symbols were calculated by assuming that $\nu(V)$ followed two different linear fits at low and higher pressure that were smoothly joined at intermediate pressure. For peaks 5, 4a, 3b, and 3a, the frequency was assumed constant at high pressure. Uncertainty in γ_i is roughly 10%. All peaks that show a linear trend of ν vs. V also can be approximated by $q =$ constant $= 1 + \gamma_i(0)$. The peaks having two different nonzero slopes for $d\nu/dV$ yield an S-shaped curve for ln γ_i vs. ln V (dot with line and circle with one bar).

0.76, whereas all but one of the mid-IR bands have $\gamma_i(0)$ of below 0.85. This difference is related to the relative compressibilities of the polyhedra. (See "Comparison of mid- and far-IR trends.") A smooth change in $\gamma_i(0)$ with frequency does not exist. The lowest $\gamma_i(0)$ values are associated with internal motions of SiO_4 tetrahedra. The highest $\gamma_i(0)$ values are associated with the bands that consist of complex motions involving both tetrahedra and octahedra. Intermediate values occur for M-O translational motions. The vibrational motion, not the energy, is the key factor in determining the mode Grüneisen parameter, although these factors are related.

IMPLICATIONS FOR BAND ASSIGNMENTS OF OLIVINE

The behavior of the bands with pressure supports the correlation of analogous IR peaks between forsterite and fayalite made by Hofmeister (1987), but not that of Kovach et al. (1975). For example, of the multicomponent bands, only bands 3 and 4 split with increasing pressure and undergo Fermi resonance (accidental degeneracy). Both minerals show essentially the same pattern of steep and shallow sloping frequencies, except that a strikingly steep band like peak 2a in forsterite was not observed in fayalite. Possibly, the peak at 200 cm^{-1} seen in the single-crystal spectra at pressure is not solely due to $B_{1u}(3)$ (peak 5) but also contains a contribution from the missing $B_{3u}(5)$ (band 7) or $B_{3u}(1)$ (band 2) (Fig. 12).

The pressure response of the various bands can also be used to evaluate the band assignments (Table 1) because
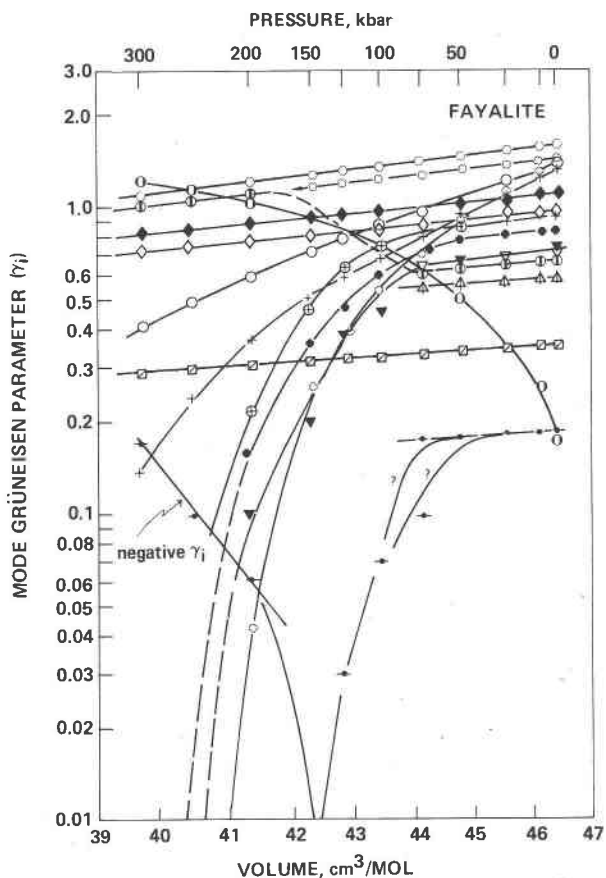
bands with similar motions should behave similarly with pressure. Bands 4, 5, 6, 8b, 9a, and 9b all were assigned to translations of M1, and all decrease in area as pressure increases and have similarly low slopes $(d\nu/dV)$. Bands 3, 7, and 8a were assigned to M2 translations, and their pressure response is similar to that of the M1 translations. Bands 1 and 2 were both assigned to SiO_4 translations; however, band 2 has a high $d\nu/dP$ and increases in area with pressure, whereas band 1 behaves similarly to the M-ion translations. This result suggests that band 1 could be a mixture of the two types of translations, whereas band 2 could be purely a translation of SiO_4 groups. Bands 3, 4, 5, and 6 are the only ones that exhibit strong curvature of frequency with volume. This implies weaker force constants as expected for the M-O bond and sug-

gests that these bands are pure M-O translations, whereas the other bands assigned to M-O translations (7, 8, and 9) are likely to be mixed with the rotational modes.

Each mid-IR band responds differently to pressure: the area of ν_4 is independent of pressure and $d\nu_4/dP$ is moderately large; the area of ν_2 is constant and $d\nu_2/dP$ is small; the area of ν_3 decreases strongly as pressure increases and $d\nu_3/dP$ is small for peak 18 and moderate for the others; ν_1 area could not be determined, whereas $d\nu_1/dP$ was small. The two rotational bands at 290 cm^{-1} in fayalite and 415 cm^{-1} in forsterite have similar slopes. Intensity information is not available on these peaks owing to the proximity of their positions to the detector's limit of operation.

The decoupling of olivine bands into internal and external modes is supported by the differences in γ_i, in that the γ_i values of the internal modes tend to be small (<1) and nearly independent of pressure, whereas γ_i values of the external modes are large (>1) and usually variable.

EVIDENCE FOR STRUCTURAL CHANGES IN OLIVINE DURING COMPRESSION

Partial and reversible transformation of α-Fe$_2$SiO$_4$ to γ-Fe$_2$SiO$_4$ is indicated by the following data: (1) New bands appear at high pressure and grow in intensity, (2) the bimodal behavior of the peak positions with pressure (i.e., several of the bands could be described as having two different constant γ_i values at high and low pressures), (3) the occurrence of mode softening in the far-IR, (4) the areas under various bands responded differently with pressure (peaks 16a and 5 grew, whereas 3c and 11 shrunk slightly, and 4a, 18, and 20 shrunk drastically). It may be that stress caused a transition, but similar behavior was seen for the hydrostatic experiments on forsterite (see below). The changes seen in the spectra suggest that the olivine structure is becoming more regular and more like spinel. The evidence is that most of the olivine bands are shrinking in intensity as is expected for a transformation to a higher symmetry; the bands that increase in area (16a and 5) are modes that also occur in spinel (i.e., ν_4 at 495 cm^{-1} and T(M) at 205 cm^{-1}: Hofmeister et al., 1986), and the peak that appeared at high pressure has a 1-atm value of 500 cm^{-1} that is also similar to ν_4 of γ-Fe$_2$SiO$_4$.

Evidence for a similar phase transition in forsterite can be seen in the hydrostatic experiments: the area of peak 3c remains constant while the area of peak 4b strongly decreases as pressure increases (Fig. 5). This behavior is markedly similar to that of fayalite under nonhydrostatic conditions (the area of peak 3c decreased slightly while that of 4b drastically shrunk). Parallel behavior also occurred in the nonhydrostatic experiments on forsterite: a new band appeared at pressure (peak 16b: Xu et al., 1983), the few bands that increased in area with pressure (2a, 9, and 16) are shared with spinel, and most of the bands decreased or stayed the same in intensity. The changes for forsterite appear less drastic because this mineral is closer to its stability field than was fayalite during the

experiments. The spectroscopic evidence is in accord with the X-ray studies at pressure of Kudoh and Takéuchi (1985) and Kudoh and Takeda (1986), which have shown that octrahedral distortion in forsterite and fayalite decreases with pressure such that changes in the structure are readily apparent above about 80 kbar.

CONCLUSIONS

IR spectroscopy at pressure is a useful tool for understanding bonding in olivine under mantle conditions. The data corroborate the band assignments based on 1-atm spectra by Hofmeister (1987). The data indicate an instability of olivine above 100–200 kbar even at room temperatures, and its consequent partial conversion to a higher-pressure structure. The response of peak area to pressure suggests that the olivine structure is gradually and reversibly altered during compression at room temperature even in the hydrostatic experiments. The proposed higher-pressure polymorph is a more regular structure than olivine and shares characteristics with the γ-spinel structure. The above observations suggest that equation-of-state data obtained near or above the stability limit may not be pertinent to the 1-atm structure.

Mode Grüneisen parameters derived from measured frequency shifts for olivine are highly dependent on the individual bands, such that internal motions of SiO$_4$ have values of $\gamma_i(0)$ generally less than unity and near zero or slightly negative values of $q_i(0)$ that weakly depend on pressure. These results can be related to the incompressibility of the Si–O bond (Hazen and Finger, 1982). The M-ion translational motions have $\gamma_i(0)$ larger than unity and large $q_i(0)$ values that often depend strongly on pressure; these are expected for the weaker M-O bonds in olivine that absorb the compression of the solid. Although the differences in bonding are readily apparent, in actuality, neither the M–O nor the Si–O bonds are very compressible, leading to small, but measurable, changes in frequency over pressure.

Negative values of q_i are possible for the majority of bands that have linear dependence of frequency on pressure. Negative values are reasonable for q_i in that the second thermal Grüneisen parameter is related to K'', γ_{th} is related to K', and frequencies are related to K, the bulk modulus (see Brout, 1959; Hofmeister, in prep.): values of K'' measured so far are small and negative (e.g., Chhabildas and Ruoff, 1976).

The observed small changes in $\nu(V)$ make exact determinations of q_i (i.e., the pressure dependence of γ_i) difficult, except for four to six bands in each mineral that show strong curvature of ν with pressure or volume. However, the data are sufficiently accurate to establish $\gamma_i(0)$ within $\pm20\%$ for all bands. The best representation is that $\gamma_i(0)$ be calculated from the average of the values derived from the two polynomial representations, $\nu(P)$ and $\nu(V)$.

For bands having cubic or quadratic dependence of ν on pressure or volume, both γ_i and q_i can be calculated reasonably accurately from the polynomial fits. The de-

parture of the second mode Grüneisen parameter from an integer for some of these bands strongly suggests that q_i should not be limited to an integer for the other bands or for other minerals. When $q_i(0)$ is greater than about six, as occurs for some of the M1 transitions, the pressure or volume dependence of q_i and the curvature of γ_i become appreciable. The strong pressure dependence of q_i for these bands suggests that assuming q_i is a constant may be inappropriate for the majority of olivine's IR bands. To the best of our knowledge, γ_i decreases by about 30% over 400 kbar for the bands exhibiting linear behavior of frequency with pressure or volume. Because it is unlikely that olivine is unique among silicates, the second Grüneisen parameter is also best represented by the average of calculations based on polynomial expansions of frequency with pressure and with volume, rather than by constant q. Using such an average allows an estimate of the accuracy of q_i to be made and takes into account the nonnegligible effect of uncertainties in the equation of state and the interdependence of γ_i and q_i.

REFERENCES CITED

Adams, D.M., and Sharma, S.K. (1978) Vibrational spectroscopy at very high pressures: XX. Raman and far-IR study of the phase transition in paratellurite. Journal of Physics and Chemistry of Solids, 39, 515–519.

Akaogi, M., Ross, N.L., McMillan, P., and Navrotsky, A. (1984) The Mg₂SiO₄ polymorphs (olivine, modified spinel and spinel)—Thermodynamic properties from oxide melt solution calorimetry, phase relations, and models of lattice vibrations. American Mineralogist, 69, 499–512.

Bassett, W.A., Shimizu, H., and Brody, E.M. (1982) Pressure dependence of elastic moduli of forsterite by Brillouin scattering in the diamond anvil cell. In S. Akimoto and M. Manghnani, Eds., High-pressure research. Academic Press, New York.

Besson, J.M., Pinceaux, J.P., Anastopoulos, C., and Velde, B. (1982). Raman spectra of olivine up to 65 kbar. Journal of Geophysical Research, 87, 10773–10775.

Brout, R. (1959) Sum rule for lattice vibrations in ionic crystals. Physical Review, 113, 43–44.

Chbabildas, L.C., and Ruoff, A.L. (1976) Isothermal equation of state for sodium chloride by the length-change-measurement technique. Journal of Applied Physics, 47, 4182–4187.

Dietrich, P., and Arndt, J. (1982) Effects of pressure and temperature on the physical behavior of mantle-relevant olivine, orthopyroxene, and garnet: 2. Infrared absorption and microscopic Grueneisen parameters.

In W. Schreyer, Ed., High pressure research in geoscience, p. 307–319. E. Schweizerbart'sche Verlagsbinchhandlung, Stuttgart.

Ferraro, J.R (1984) Vibrational spectroscopy at high external pressures: The diamond-anvil cell. Academic Press, New York.

Ferraro, J.R., Mitra, S.S., and Postmus, C. (1966) The far-infrared spectra of solids under high pressure (33–100μ). Inorganic and Nuclear Chemical Letters, 2, 269–275.

Ferraro, J.R., Postmus, C., Mitra, S.S., Hoskins, C., and Siwiec, E.C. (1970) Optical phonons of ZnS₁₋ₓSeₓ and CdS₁₋ₓSeₓ mixed crystals: Pressure effects. Applied Spectroscopy, 24, 187–192.

Ferraro, J.R., Horan, H., and Quattrochi, A. (1971a) Pressure dependence of the infrared-active optical phonon modes in alkaline-earth fluorides. Journal of Chemical Physics, 55, 664–666.

Ferraro, J.R., Mitra, S.S., and Quattrochi, A. (1971b) Pressure dependence of infrared eigenfrequencies of KI, RbI, and their mixed crystals. Journal of Applied Physics, 42, 3677–3681.

Graham, E.K., Jr., and Barsch, G.R. (1969) Elastic constants of single-crystal forsterite as a function of temperature and pressure. Journal of Geophysical Research, 74, 5949–5960.

Graham, E.K., Jr., Schwab, J.A., Sopkin, S.M., and Takei, H. (1988) The pressure and temperature dependence of the elastic properties of single-crystal fayalite Fe₂SiO₄. Physics and Chemistry of Minerals, 16, 186–198.

Hazen, R.M., and Finger, L.W. (1982) Comparative crystal chemistry: Temperature, pressure, composition, and the variation of the crystal structure. Wiley, New York.

Hofmeister, A.M. (1987) Single-crystal absorption and reflection infrared spectroscopy of forsterite and fayalite. Physics and Chemistry of Minerals, 14, 499–513.

Hofmeister, A.M., Mao, H.K., and Bell, P.M. (1986) Spectroscopic determination of thermodynamic properties of γ-Fe₂SiO₄ at mantle pressures. EOS, 67, 395.

Iishi, K. (1978) Lattice dynamics of forsterite. American Mineralogist, 63, 1198–1208.

Jephcoat, A.P., Mao, H.K., and Bell, P.M. (1986) Static compression of iron to 78 GPa with rare gas solids as pressure-transmitting media. Journal of Geophysical Research, 91, 4677–4684.

Kauppinen, J.K., Moffatt, D.J., Mantsch, H.H., and Cameron, D.G. (1981) Fourier self-deconvolution: A method for resolving intrinsically overlapped bands. Applied Spectroscopy, 35, 271–276.

Kieffer, S.W. (1979a) Thermodynamics and lattice vibrations of minerals: 1. Mineral heat capacities and their relationships to simple lattice vibrational models. Reviews of Geophysics and Space Physics, 17, 1–19.

——— (1979b) Thermodynamics and lattice vibrations of minerals: 2. Vibrational characteristics of silicates. Reviews of Geophysics and Space Physics, 17, 20–34.

——— (1979c) Thermodynamics and lattice dynamics of minerals: 3. Lattice dynamics and an approximation for minerals with application to simple substances and framework silicates. Reviews of Geophysics and Space Physics, 17, 35–59.

——— (1980) Thermodynamics and lattice vibrations of minerals: 4. Application to chain and sheet silicates and orthosilicates. Reviews of Geophysics and Space Physics, 18, 862–886.

——— (1982) Thermodynamics and lattice vibrations of minerals: 5. Applications to phase equilibria, isotopic fractionation, and high-pressure thermodynamic properties. Reviews of Geophysics and Space Physics, 20, 827–849.

Kovach, J.J., Hiser, A.L., and Karr, C., Jr. (1975) Far-infrared spectroscopy of minerals. In C. Karr, Jr., Ed., Infrared and raman spectroscopy of lunar and terrestrial minerals, p. 231–254. Academic Press, New York.

Kudoh, Y., and Takeda, H. (1986) Single crystal X-ray diffraction study on the bond compressibility of fayalite Fe₂SiO₄ and rutile TiO₂ under high pressure. Physica, 140B, 333–336.

Kudoh, Y., and Takéuchi, Y. (1985) The crystal structure of forsterite Mg₂SiO₄ under high pressure up to 149 kb. Zeitschrift für Kristallographie, 171, 291–302.

Kumazawa, M., and Anderson, O.L. (1969) Elastic moduli, pressure derivatives, and temperature derivatives of single-crystal olivine and single-crystal forsterite. Journal of Geophysical Research, 74, 5961–5972.

Lees, A.C., Bukowinski, M.S.T., and Jeanloz, R. (1983) Reflection prop-

erties of phase-transition and compositional-change models of the 670-km discontinuity. Journal of Geophysical Research, 88, 8145–8159.

Lowndes, R.P., and Rastogi, A. (1976) Temperature and pressure dependence of the transverse-optic modes of ionic crystals and their associated anharmonic self-energies. Physical Review, B14, 3598–3620.

Mao, H.K., and Bell, P.M. (1978) Design and varieties of the megabar cell. Carnegie Institution of Washington Year Book 77, 904–913.

Mao, H.K., Bell, P.M., Shaner, J.W., and Steinberg, J.D. (1978) Specific volume measurements of Cu, Mo, Pd, and Ag and the calibration of the ruby R_1 fluorescence pressure gauge from 0.06 to 1 Mbar. Journal of Applied Physics, 49, 3276–3283.

Mao, H.K., Hadidiacos, C.G., Bell, P.M., and Goettel, K.A. (1983) Automated system for heating and for spectral measurements in the diamond-window, high-pressure cell. Carnegie Institution of Washington Year Book 82, 421–424.

Mao, H.K., Xu, J., and Bell, P.M. (1986) Calibration of the ruby pressure gauge to 800 kbar under quasi-hydrostatic conditions. Journal of Geophysical Research, 91, 4673–4676.

Moller, K.D., and Rothschild, W.G. (1970) Far-infrared spectroscopy. Wiley, New York.

Servoin, J.L., and Piriou, B. (1973) Infrared reflectivity and Raman scattering of Mg_2SiO_4 single crystal. Physica Status Solidi, 55, 677–686.

Shawyer, M.S., and Sherman, W.F. (1982) The pressure dependence of alkali halide TO mode frequencies. Modern Physics, 22, 23–29.

Sherman, W.F. (1982) Infrared and Raman spectroscopy at high pressures. Journal of Molecular Structure, 113, 101–116.

Webb, S.L., Jackson, I., and Takei, H. (1984) On the absence of shear mode softening in single-crystal fayalite Fe_2SiO_4 at high pressure and room temperature. Physics and Chemistry of Minerals, 11, 167–171.

Xu, J., Mao, H.K., Weng, K., and Bell, P.M. (1983) High-pressure Fourier-transform infrared spectra of forsterite and fayalite. Carnegie Institution of Washington Year Book 82, 350–352.